JOURNAL OF GEOPHYSICAL RESEARCH, VOL. 100, NO. B7, PAGES 12,791–12,811, JULY 10, 1995

Compressive and tensile failure of inclined well bores and determination of in situ stress and rock strength

Pavel Peška[1] and Mark D. Zoback

Department of Geophysics, Stanford University, Stanford, California

Abstract. In this paper we investigate the occurrence of compressive and tensile failures of arbitrarily inclined well bores under a wide variety of stress conditions. The principal assumptions in this analysis are that the rock is isotropic and that it deforms elastically to the point of failure. As has been shown by previous investigators, for a given stress state and well bore orientation, it is straightforward to predict the orientation of the failures around the well bore as well as whether failure is likely to occur depending on such parameters as rock strength and borehole fluid pressure. However, as the stress state is almost never known in situ, we demonstrate how observations of compressive and tensile wall failures in inclined holes can be used to constrain in situ stress orientations and magnitudes if there are independent data on the magnitude of the least principal stress from either leak-off or microfrac tests and on the formation pore pressure. We further demonstrate how once the stress state is determined, it is possible to assess both an upper bound on the effective in situ rock strength and the degree to which increasing the borehole fluid pressure (or mud weight) can reduce the likelihood of borehole failure. Through application of this methodology to an inclined well bore in an area of complex faulting in the Gulf of Mexico, we illustrate how it is possible to utilize observations of borehole failures to determine the magnitude and orientation of the stress tensor in areas such as offshore sedimentary basins where drilling inclined well bores is quite common.

Introduction

It is well known that when a borehole is drilled, the rock surrounding the hole must carry the forces previously carried by the removed rock and a stress concentration is produced around the borehole [*Kirsch*, 1898]. If the stress concentration exceeds rock strength, failure can occur in either compression or tension. Stress-induced compressive well bore failures are commonly known as well bore breakouts (Figure 1), [e.g., *Bell and Gough*, 1979; *Zoback et al.*,1985; *Plumb and Hickman*, 1985] and can be observed with either four-arm caliper logs or borehole televiewers. Tensile well bore fractures can also occur around a well bore under certain stress conditions [*Aadnoy*, 1990b; *Brudy and Zoback*, 1993]. While drilling-induced hydraulic fractures are well known in the petroleum industry and can be quite problematic because they are associated with lost circulation [e.g., *Stock et al.*, 1985; *Moos and Morin*, 1991], the tensile well bore fractures we are referring to are very small-scale features that occur in the rock immediately adjacent to the well bore and can be detected only through detailed well bore imaging using devices such as the formation microscanner/microimager (FMS/FMI) logging [e.g., *Ekstrom et al.*, 1987]. We term these features tensile wall fractures as they occur only in the wall of the borehole due to stress concentration and do not propagate away from the borehole. Plate 1 shows two examples of such fractures [after M. Brudy, personal communication, 1994; *Zoback et al.*, 1993]. These fractures form either parallel to the borehole axis (Plate 1a) or in en echelon "chevron" patterns where the fracture planes are inclined to the borehole axis (Plate 1b). The case of "chevron" patterns has been interpreted by *Brudy and Zoback* [1993] to indicate a case in which the borehole axis is not parallel to one principal stress.

In recent years the stability of deviated boreholes has been of particular interest in petroleum industry [e.g., *Cooper*, 1994]. In drilling such holes a major operational concern is the prevention of borehole wall failure. Various authors have addressed different aspects of this problem in the past. *Bradley* [1979] and *Aadnoy and Chenevert* [1987] developed linear elastic models for compressive and tensile failure of an inclined borehole which can be used to select proper mud weights to prevent borehole failure. *Daneshy* [1973], *Richardson* [1981], *Yew and Li* [1988], *Roegiers and Detournay* [1988], and *Baumgärtner et al.* [1989] have done numerical and experimental analyses of hydraulic fractures in inclined holes, whereas *Rawlings et al.* [1993] studied formation of breakouts in inclined boreholes. Although these studies take into account the effect of a far-field tectonic stress field in which one principal stress is not aligned with the borehole axis, only the results for specific borehole orientations and stress states were considered. In this paper, we present a systematic analysis of borehole stability (including both compressive and tensile failures) for arbitrarily inclined boreholes in a wide variety of stress states ranging from extensional tectonic environments to highly compressional ones. Moreover, we consider the likelihood of compressive and tensile borehole failure as a function of rock strength and borehole fluid pressure over a wide range of conditions.

Our other motivation for comprehensively analyzing compressive and tensile failures in inclined boreholes is to utilize this information to assess the orientation and magnitude of the stress tensor in situ. Well bore breakouts and tensile fractures in vertical

[1] Also at Geophysical Institute, Academy of Sciences of the Czech Republic, Prague.

Paper number 95JB00319.
0148-0227/95/95JB-00319$05.00

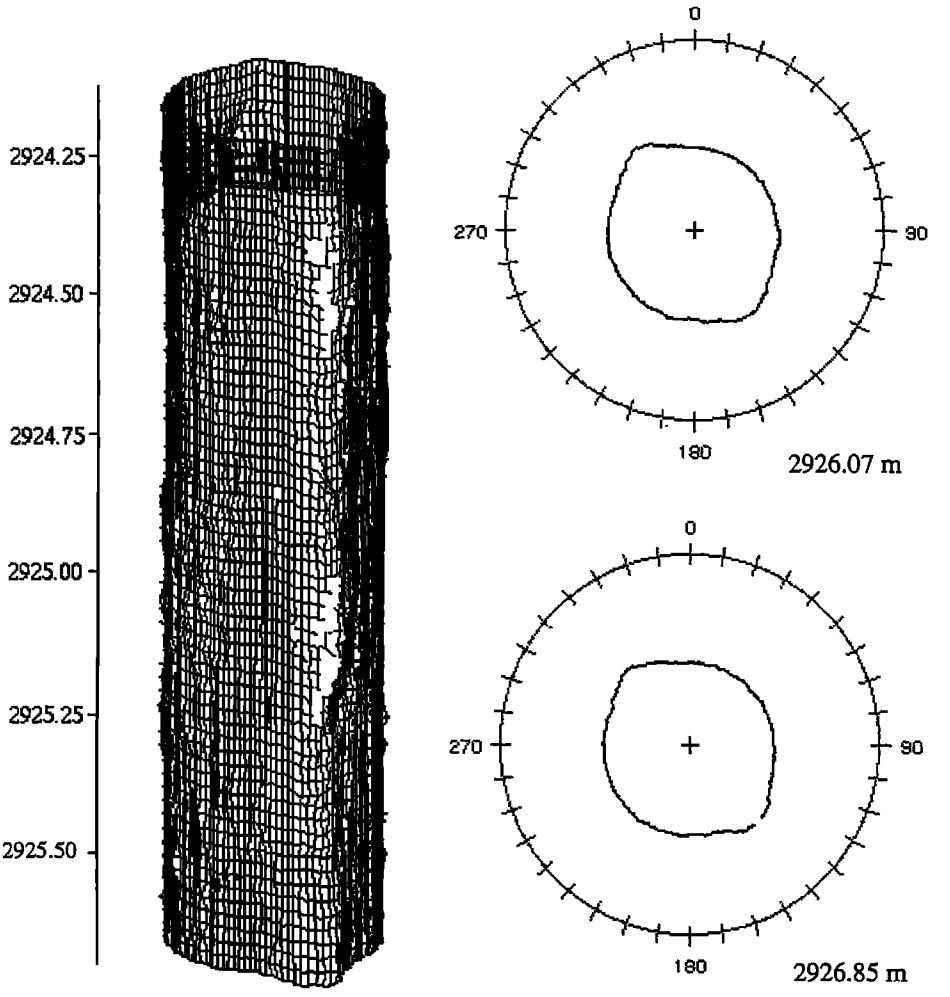

Figure 1. Example of stress-induced borehole breakouts seen as enlargements of the borehole wall (left) in a cylindrical relief view and (right) in polar cross sections of the hole (Kent Cliffs borehole, New York).

boreholes are reliable indicators of the orientation of principal stress directions when one principal stress is vertical (see, for example, the compilations of in situ stress data by *Bell and Gough* [1979], *Gough and Bell* [1981], *Zoback and Zoback* [1980, 1989, 1991], *Plumb and Cox* [1987], *Zoback et al.* [1989], *Adams and Bell* [1991], *Müller et al.* [1992], and *Zoback* [1992]). These compilations do not include observations of failures in inclined boreholes because (1) four-arm caliper logs (typically used to study breakouts) do not easily distinguish between breakouts and "key seats" in inclined holes caused by mechanical erosion of the well bore wall [*Plumb and Hickman,* 1985] and (2) breakout directions in inclined holes can deviate significantly from what is predicted for vertical holes [e.g., *Mastin,* 1988]. Because of these potential problems it has been typical to ignore data from inclined holes when assessing in situ stress orientations. In this paper we take the opposite approach. Because inclined holes are drilled so frequently in the petroleum industry (especially off shore) there are many instances in which it is quite important to assess the stress state in the vicinity of such holes. Further, we show that the details of failure of inclined holes are sensitive to the exact stress conditions so that the study of such failures can provide important insight into stress orientations and magnitudes.

Several authors have addressed the subject of the relationship between the failure of inclined holes and the tectonic stress field. *Mastin* [1988] demonstrated that breakouts in inclined holes drilled at different azimuths were expected to form at various angles around a well bore. *Qian and Pedersen* [1991] proposed a nonlinear inversion method to attempt to extract information about the in situ stress tensor from breakouts in an inclined deep borehole in the Siljan impact structure in Sweden. *Qian et al.* [1994] later presented a correction of their results because of errors in the published equations of *Mastin* [1988] (although the figures in Mastin's paper are correct). *Zajac and Stock* [1992] suggested in a published abstract that it is possible to constrain stress magnitudes from breakout azimuths if there are observations from a number of inclined holes drilled at various azimuths in a uniform stress field. This technique is conceptually similar to a technique reported by *Aadnoy* [1990a,b] to estimate in situ stress from hydraulic fracturing data in a number of inclined boreholes.

However, because data from multiple inclined boreholes in a uniform stress field may not often be available, in this paper we focus on what can be learned from an integrated analysis of different types of well bore failure in a single inclined hole. Further, we examine the relationships between both compressive and tensile failure of inclined holes and the tectonic stress field and attempt to take into account all representative stress conditions which may be encountered in different parts of the world with the objectives (1) to develop improved methods to constrain

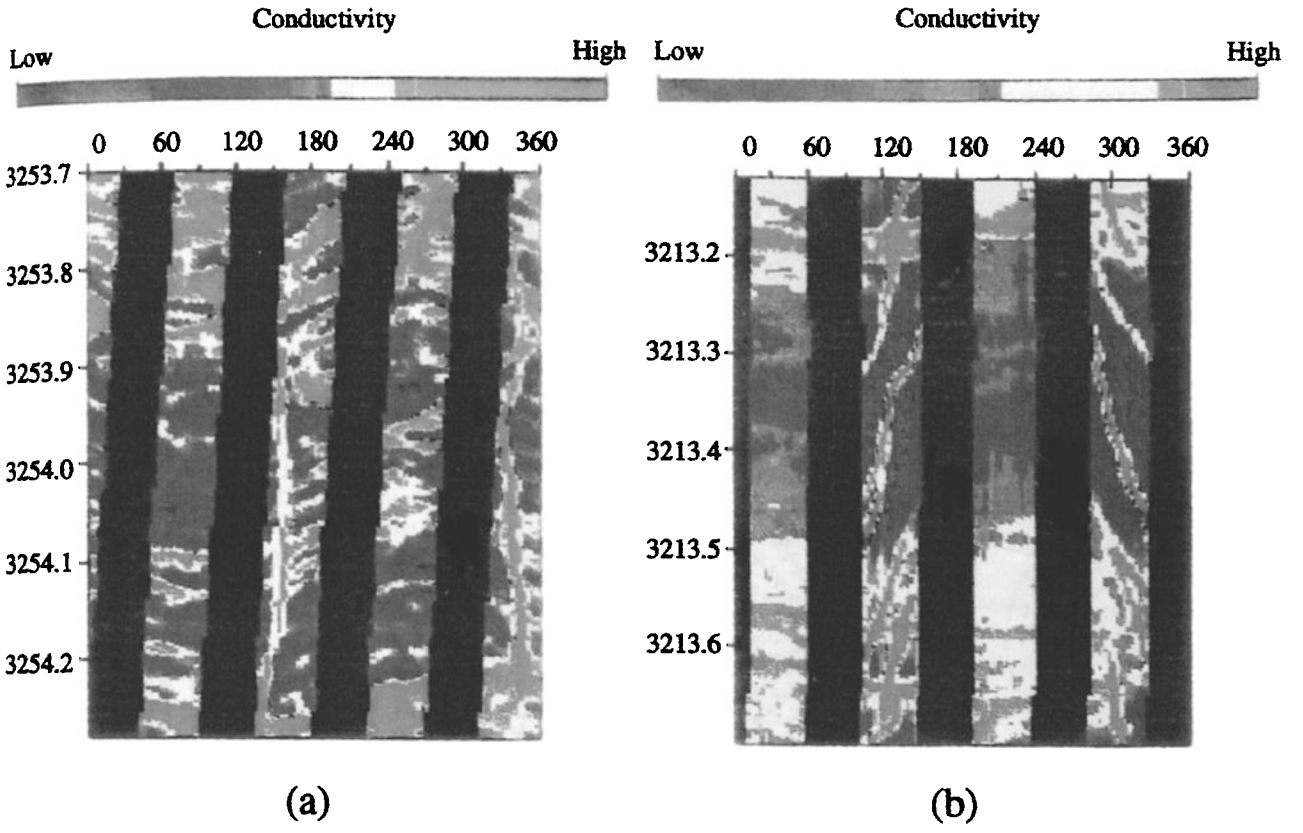

Plate 1. A fine-scale electrical conductivity image (FMS image) of the inside of the borehole wall showing (a) a near-vertical drilling-induced tensile fracture cut across foliation planes in the rock [after *Zoback et al.*, 1993], and (b) en echelon "chevron" pattern of fine wall fractures which are inclined to the borehole axis (after M. Brudy, personal communication, 1994).

both the stress tensor and rock strength utilizing information on failure of deviated holes and (2) to contribute to the practical problem of understanding borehole stability in tectonically stressed areas (to determine the most stable and unstable directions of drilling, to estimate optimal mud weights to prevent borehole failure, etc.).

In the first part of the paper we discuss these subjects in a very generalized manner making a number of assumptions about in situ stress, rock strength, and other parameters, simply to illustrate the effects of various parameters on borehole stability. At the end of the paper we present a case in which we apply the theory developed in the paper to data collected in an inclined well in the Gulf of Mexico and illustrate that making relatively few assumptions about the stress field and the types of data commonly available in inclined wells it is possible to estimate both the orientation and magnitude of the stress tensor and to place bounds on the effective rock strength.

Method to Present Orientation of Failure and Borehole Stability

The following analysis is based on the assumption of linear elastic behavior of an homogeneous isotropic rock up to the point of failure. For an arbitrarily oriented borehole (Figure 2), the effective principal stresses at the borehole wall are given by

$$\sigma_{t\max} = \frac{1}{2}[\sigma_{zz} + \sigma_{\theta\theta} + \sqrt{(\sigma_{zz} - \sigma_{\theta\theta})^2 + 4\tau_{\theta z}^2}]$$
$$\sigma_{t\min} = \frac{1}{2}[\sigma_{zz} + \sigma_{\theta\theta} - \sqrt{(\sigma_{zz} - \sigma_{\theta\theta})^2 + 4\tau_{\theta z}^2}] \quad (1)$$
$$\sigma_{rr} = \Delta P$$

where ΔP is the difference between the borehole fluid pressure and the pore pressure in the rock (differential mud weight) and σ_{zz}, $\sigma_{\theta\theta}$, $\tau_{\theta z}$ are effective stresses in the borehole cylindrical

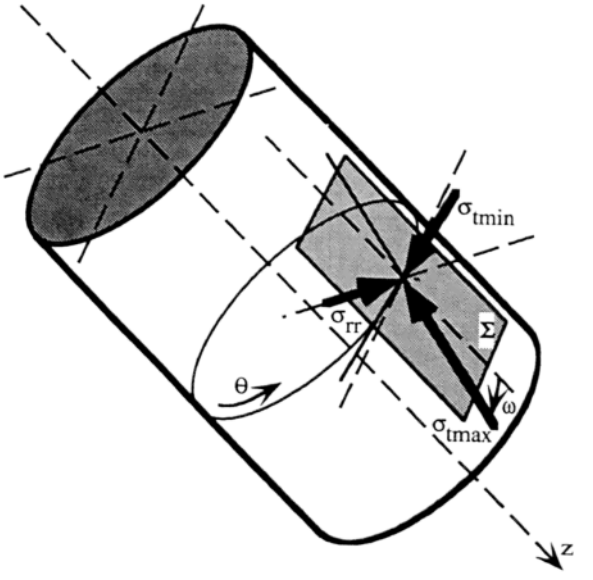

Figure 2. Principal stresses $\sigma_{t\max}$, $\sigma_{t\min}$, and σ_{rr} at the wall of an inclined borehole for a point oriented at angle θ measured from the bottom side of the hole. $\sigma_{t\max}$ and $\sigma_{t\min}$ act in a plane tangent to the borehole (plane Σ), while σ_{rr} acts normal to this plane. The maximum tangential stress, $\sigma_{t\max}$, deviates by an angle ω from the borehole axis.

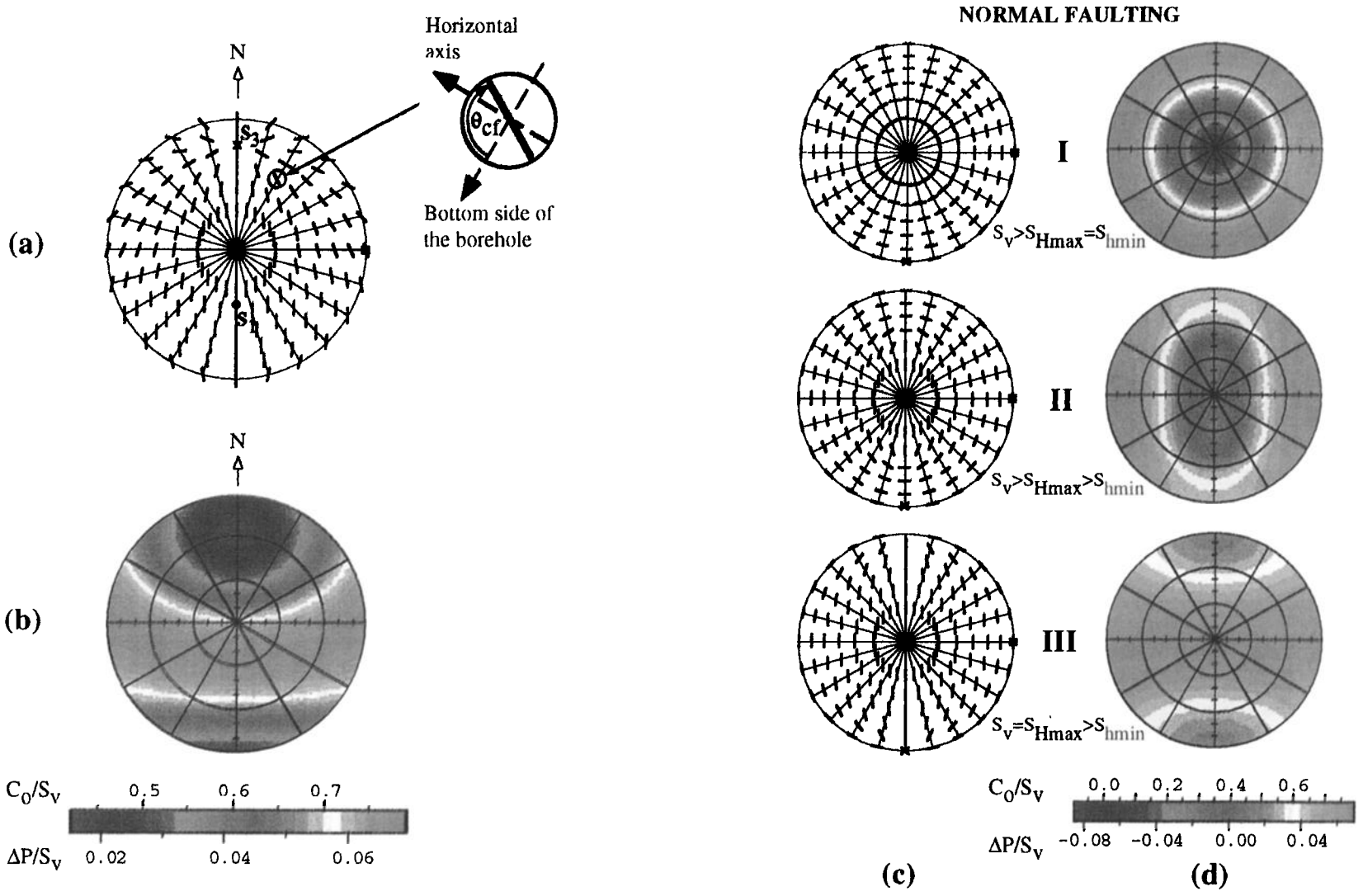

Plate 2. Breakouts in deviated boreholes: method of presentation (Plates 2a and 2b) and breakouts in the normal faulting stress regime (Plates 2c and 2d). (a) Breakout directions (plotted using the "looking down the hole" convention) for boreholes of various orientations and given far-field principal stresses S_1, S_2, S_3. The angle of failure, θ_{cf}, is measured clockwise from the bottom side of the hole in the plane perpendicular to the borehole axis (see detail). (b) Tendency for breakouts to occur as a function of normalized rock strength, C_0/S_v (computed for $\Delta P = 0.1\ S_v$) or differential mud weight, $\Delta P/S_v$ (for $C_0 = S_v$) necessary to prevent borehole failure. A hydrostatic pore pressure, $P_p = 0.45\ S_v$, and $\mu_i = 1$ are assumed. (c) Breakout orientations and (d) tendency for failure of inclined boreholes in the normal faulting stress regime. Stress states correspond to the states of stress I-III from Figure 3. $S_{H\max}$ acts from left to right; $S_{h\min}$ acts from top to bottom at each polar plot. The tendency for failure is expressed as a function of differential borehole fluid pressure, ΔP (computed for $C_0 = S_v$ and $\mu_i = 1$) or effective rock strength, C_0 (for $\Delta P = 0.1\ S_v$ and $\mu_i = 1$) which is necessary to prevent borehole failure.

coordinate system (Figure A1). The complete equations are given in Appendix A. Since one principal stress, the radial stress σ_{rr}, is always perpendicular to the borehole wall, the other two, maximum and minimum tangential stresses $\sigma_{t\max}$ and $\sigma_{t\min}$, act in a plane tangential to the borehole wall (plane Σ in Figure 2) and they deviate by angles ω and $\omega + 90^{\circ}$, respectively, from the borehole axis, where

$$\tan 2\omega = \frac{2\tau_{\theta z}}{\sigma_{zz} - \sigma_{\theta\theta}} \quad . \tag{2}$$

Equations (1) reduce to the simple *Kirsch* [1898] equations if one principal stress direction coincides with the borehole axis.

The borehole stress state (1) is a function of the tectonic stresses S_1, S_2, S_3 (Appendix A). It is important to illustrate the conditions for borehole failure under the wide range of the stress states that may be encountered in different parts of the world. In extensional regions, principal stresses that are approximately horizontal ($S_{H\max}$ and $S_{h\min}$) may be considerably less than the vertical stress (S_v), whereas in highly compressional areas the opposite is true [*Anderson*, 1937]. To consider the full range of possible stress states over the world, but to limit the number of illustrative figures, we assume that one of the principal stresses is vertical and that the state of stress within the crust is in frictional equilibrium, in which case the ratio of effective principal stresses is given by *Jaeger and Cook* [1979] as

$$\frac{S_1 - P_p}{S_3 - P_p} = \left(\sqrt{\mu^2 + 1} + \mu\right)^2 \tag{3}$$

where μ is the coefficient of frictional sliding on preexisting planes of weakness ($0.6 < \mu < 1.0$ [*Byerlee*, 1978]) and P_p is the in situ pore pressure. While we believe it is likely that (3) is valid in holes drilled in many parts of the world (see discussions by *Zoback and Healy* [1984, 1992]), the stress states prescribed by (3) below for different tectonic environments are assumed only for the purpose of illustrating the effect of markedly different stress states on borehole stability. The possible values of $S_{H\max}$ and $S_{h\min}$ defined by (3) can be easily portrayed in a polygonally shaped region (Figure 3, following *Moos and Zoback* [1990, 1993]) that defines the stresses allowable by frictional strength of the crust at any given depth. Stress states in which the crust is in frictional equilibrium (as given by equation (3)) correspond to the points lying at the periphery of the polygon for tectonic regimes. Such states can vary between the highly extensional stress state I (in which $S_{H\max} = S_{h\min} << S_v$) and highly compressional stress state VII (in which $S_{H\max} = S_{h\min} >> S_v$). It follows from Figure 3 that for hydrostatic pore pressure, $P_p = 0.45\ S_v$, and $\mu = 0.6$, the horizontal stresses must fall in the range $0.63\ S_v \leq S_{h\min}$, $S_{H\max} \leq 2.17\ S_v$. For higher pore pressures, lower coefficients of friction, or stress states that depart from frictional equilibrium, a smaller range of differential stress values may exist.

The stress state at the borehole wall is fully determined by the three principal stresses (1) which control the mode and orientation of the borehole failure. The stresses around the well bore are functions of 11 parameters (see Appendix A). Six of them describe the stress tensor (e.g., three magnitudes of principal stresses and three Eulerian angles determining their orientation), two describe the borehole geometry (azimuth and inclination), and the last three are Poisson's ratio of the rock, the differential borehole fluid pressure, and the angle which determines the

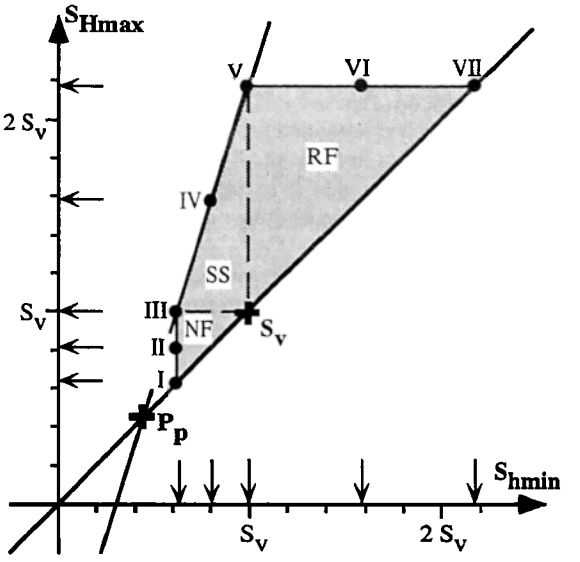

Figure 3. Allowable horizontal stresses $S_{H\max}$ and $S_{h\min}$ in the crust based on the frictional strength of favorably oriented fault planes. Points at the periphery of the polygon (e.g., points I-VII) correspond to a state of stress at the frictional limit. For the case shown, the pore pressure is assumed to be hydrostatic, $P_p = 0.45\ S_v$, and the frictional coefficient is $\mu = 0.6$. NF, the normal faulting stress regime; SS, the strike-slip regime; and RF, the reverse faulting stress regime. Stress values are normalized by the vertical stress S_v (weight of the overburden) to make the analysis independent of depth.

position around the borehole wall (Figure 2). As the number of parameters in the analysis is large, it is important to utilize an efficient method to present the results of the analysis as we assess the significance of the many parameters. *Mastin* [1988] presented spatial orientations of the boreholes and breakouts in a lower hemisphere stereographic projection. We follow this approach to present any borehole and stress tensor in a lower hemisphere spherical projection (Plate 2a). A vertical borehole is in the center of each circular plot, and horizontal holes lie at the periphery. Arbitrarily oriented holes are shown as a function of their inclination with respect to vertical (radial distance from the center) and azimuth measured clockwise from the north. In all subsequent figures, we show boreholes which deviate from vertical at increments of 15° and at azimuths varying by 15° increments.

For a given stress state, Plate 2a illustrates the direction of well bore failures (in this case breakouts; tensile wall fractures are discussed below) assuming that they occur, for a case where S_1, the maximum principal stress deviates 25° to the south from the vertical, S_2, the intermediate principal stress acts horizontally in an E-W direction, and S_3 acts N-S but is also inclined 25° (see the symbols in Plate 2a; the in situ stress tensor is defined by effective stress magnitudes of $\sigma_1 = \sigma_2 = 3.12\ \sigma_3$ and Eulerian angles $\alpha = 0^{\circ}$, $\beta = 65^{\circ}$, $\gamma = 0^{\circ}$). In contrast to *Mastin's* [1988] projection of breakout orientations onto a horizontal plane, breakout directions around the hole are plotted as if the reader is viewing the hole by looking down its axis. For example, the detailed illustration in Plate 2a is intended to show the orientation of breakouts in a borehole inclined 45° from vertical in the direction N30°E. In this case, the short line segment in the spherical projection illustrates that the breakouts tend to occur

roughly along the upper left and lower right parts of the inclined hole at the angle θ_{cf} measured clockwise from the bottom side of the hole in a plane perpendicular to the hole axis (see also Figure A2 in Appendix A). We use this convention of "looking down the hole" because it is possible to easily present and visualize the orientation of failures in holes of all orientations, even in nearly horizontal holes when the failures occur at the top and bottom of the hole and the orientation of failure cannot be projected onto a horizontal plane.

To consider whether breakouts are likely to occur in wells of varied orientation and in different stress states, it is also necessary to consider rock strength, formation pore pressure, and pressure in the well bore and to present these data in a visually convenient form. For the same stress magnitudes and orientations used in Plate 2a, Plate 2b shows the tendency for compressive well bore failure to occur as a function of rock strength and differential borehole fluid pressure (the difference between the well bore fluid pressure and the in situ pore pressure). Again the results are presented in lower hemisphere representations of different borehole orientations. All values of rock strength and differential fluid pressure are normalized by the overburden stress to make the analysis depth independent. The colors in Plate 2b show the tendency for failure to initiate (red is most likely to fail and blue is least likely) as a function of either differential fluid pressure in the well bore or in situ rock strength (which corresponds to the in situ strength of the rock under the polyaxial stress conditions existing at the borehole wall [e.g., *Aadnoy and Chenevert*, 1987; *Vernik and Zoback*, 1992]. For simplicity, we have assumed a linear Mohr-Coulomb failure law in this analysis with a coefficient of internal friction, μ_i, and uniaxial compressive strength, C_0 (Appendix B), but other failure criteria could be incorporated as well.

The way in which to interpret Plate 2b quantitatively is that the color corresponds to the minimum value of rock strength or differential mud weight required to inhibit failure (Figure B1 indicates the method of computation). In other words, the red colors indicate hole orientations in which failure is expected to occur in relatively strong rock or despite relatively high differential mud weight. Specifically, the region in Plate 2b shown in red indicates that unless the uniaxial rock strength C_0 exceeds about $0.75S_v$, failure is likely to occur, whereas holes oriented in directions indicated by blue colors indicate failure is unlikely even in rock with considerably lower strength ($C_0/S_v \sim 0.55$). Similarly, if one were attempting to prevent borehole failure by increasing the differential mud weight, the red region in Plate 2b shows that $\Delta P/S_v$ would have to exceed 0.06 to inhibit failure if $C_0/S_v \sim 1.0$. As pore pressure is 0.45 of the vertical stress (approximately hydrostatic), this means that a ~13% increase of mud weight over the pore pressure is required to prevent failure, whereas holes with orientations corresponding to blue colors require lower differential mud weight of about 0.03 S_v (~7%) to inhibit failure.

Examples of Well Bore Breakouts in Inclined Boreholes

We discuss below the basic stress states I-VII defined in Figure 3 which means that the principal stresses are assumed to act vertically and horizontally and pore pressure at depth is hydrostatic. Of course, this need not be the case in situ. These assumptions are made to isolate the effects of stress magnitudes, rock strength, and borehole fluid pressure on breakouts in a straightforward manner. We also consider below separately a case in which we vary in situ pore pressure. In Plates 2c and 2d (and all subsequent figures similar to them), we assume $S_{H\max}$, the maximum horizontal compressive stress acts from "left to right" and $S_{h\min}$ acts from "top to bottom".

For various states of stress in frictional equilibrium, Plates 2c, 2d and 3 display both the orientation of breakouts assuming that they occur, as well as tendency for breakouts to occur as a function of rock strength and borehole fluid pressure for various borehole orientations. Plates 2c and 2d show this for a normal faulting tectonic environment (cases I-III in Figure 3), Plates 3a and 3b show the same information for the case of a strike slip faulting environment (cases III-V), and Plates 3c and 3d show this for a reverse faulting environment (cases V-VII). Because the ratio between the maximum and minimum effective stress is assumed to be determined by equation (3), the different cases presented in these figures show the dependence of breakout orientation on the magnitude of the intermediate principal stress ($S_{H\max}$ for the case of normal faulting, S_v for the case of strike-slip faulting, and $S_{h\min}$ for the case of reverse faulting).

Breakout Orientations

Several conclusions about the dependence of breakout orientations on hole orientation and stress magnitude can be observed in Plates 2c, 3a and 3c which are in basic agreement with those of *Mastin* [1988]. In the least compressive case I (when the two horizontal stresses are equal and less than the vertical stress (Plate 2c)), breakouts always form on the sides of an inclined borehole regardless of hole orientation. As the difference between the horizontal stresses grows in normal faulting areas (cases II and III) holes slightly inclined in the direction close to $S_{h\min}$ tend to have breakouts at the top and bottom side of the borehole (i.e., in the direction of $S_{h\min}$ as is the case for vertical holes), whereas near-horizontal holes tend to have breakouts on the sides. Note, however, that the transition from breakouts oriented along the top and bottom to breakouts located on the sides of the hole depends on hole azimuth, inclination, and relative magnitude of the intermediate principal stress $S_{H\max}$. This suggests that in the quite common case of a hole with a constant azimuth close to that of $S_{h\min}$ and increasing inclination with depth, there are marked differences in how breakout orientations change with inclination (or depth) depending on the magnitude of $S_{H\max}$.

In a strike-slip faulting environment (Plates 3a and 3b) the breakouts in holes of low inclination have a relatively stable direction (parallel to $S_{h\min}$), whereas in steeply inclined holes the breakout direction is a strong function of hole orientation and the magnitude of the intermediate principal stress S_v (note that case III is the same in Plates 2c and 3a as it represents a transitional strike-slip/normal faulting stress state).

In reverse faulting environments (cases V-VII in Plates 3c and 3d), the breakout direction is also highly dependent on hole orientation and relative magnitude of the intermediate principal stress $S_{h\min}$ (again case V is the same as that in Plate 3a as this represents the transitional strike-slip/reverse faulting stress state). Note that there is an increasing tendency for breakouts to occur along the top and bottom of the hole with increasing values of $S_{h\min}$, which might make it difficult to distinguish between breakouts and key seats if only caliper data were available [e.g., *Plumb and Hickman*, 1985]. In the limiting compressional case where both horizontal stresses are equal and much greater than the vertical stress (case VII), breakouts always form at the top and bottom of the hole regardless of hole orientation. In both the

normal and reverse faulting cases the greatest changes in breakout orientation with inclination occur in the boreholes deviated in the plane perpendicular to the intermediate stress [see *Mastin*, 1988]. These borehole azimuths are the most sensitive to the intermediate stress, and along them, there is a specific borehole inclination for which the breakouts abruptly change orientation to a perpendicular direction. This critical inclination decreases as the horizontal stresses become more subequal [*Peska*, 1994].

Tendency for Compressive Failure to Occur

As mentioned above, Plates 2c, 3a, and 3c indicate only theoretical breakout orientations if they occur in a given well bore. Plates 2d, 3b, and 3d express the tendency for failure as a function of differential borehole fluid pressures, ΔP, and uniaxial rock strength, C_0. All values are normalized by the vertical stress for generality (and to make the results independent of depth). As in Plate 2b, for a specific borehole orientation the color indicates either the value of normalized differential borehole fluid pressure, $\Delta P/S_v$ or normalized rock strength, C_0/S_v necessary to prevent borehole failure. Thus "hot" colors (red-yellow) indicate unstable borehole orientations because relatively high borehole pressures (mud weights) or rock strengths are necessary to prevent failure. The most stable borehole orientations are shown by "cold" colors (blue) as these holes are stable even in relatively weak rocks or with little or no excess differential borehole fluid pressure. Note that the color scaling for Plates 2d, 3b, and 3d is not the same, as borehole failure is much more likely for highly compressive stress regimes than for extensional regimes.

Computations for Plates 2d, 3b, and 3d were based on the Mohr-Coulomb failure criterion (Appendix B) when the strength of the rock is controlled by the coefficient of internal friction, μ_i, and by the uniaxial strength, C_0. No attempt is made in this paper to consider the likelihood of failure for different failure criterion such as, for example, the Drucker-Prager [e.g., *Bradley*, 1979] or the Wiebols-Cook criterion [*Vernik and Zoback*, 1992]. In addition, we assume linear elastic behavior of the rock up to the point of failure and no elasto-plastic effect of strain hardening is embedded (e.g., *Veeken et al.* [1989] or *Papanastasiou et al.* [1994]). Although the elastic/brittle Mohr-Coulomb model may quantitatively differ in values of particular parameters (it leads to underestimations of stresses required to fail a borehole [e.g., *Rawlings et al.*, 1993; *Veeken et al.*, 1989]), we consider it to be adequate to illustrate in a relatively simple way the tendency for failure of arbitrarily oriented boreholes under a variety of stress conditions. For the purpose of the discussion here we consider only whether failure is likely to occur as a function of rock strength and differential mud weight. As mentioned above, one can replace the Mohr-Coulomb criterion with any other criterion if so desired.

For the cases shown in Plates 2d, 3b, and 3d we assume μ_i = 1.0 (for most rocks, μ_i is in the range $1.0 < \mu_i < 2.0$). To consider the manner in which differential mud weight can inhibit borehole failure, we assume a constant strength $C_0 = S_v$. To evaluate how important rock strength is on failure, we assume a moderate degree of differential mud weight, $\Delta P = 0.1\ S_v$. Again, these assumptions are made only for the purpose of illustration as the analysis is completely general and values appropriate to other examples can be used in application of the theory (see below). Note that for hydrostatically pressurized sedimentary rock with a density of about 2300 kg/m^3, $\Delta P/S_v = 0.1$ corresponds to a ~22% increase in borehole pressure above pore pressure.

For normal faulting stress states, Plate 2d shows that as the magnitude of the intermediate principal stress $S_{H\max}$ increases, vertical holes become more unstable, whereas the opposite is true for holes drilled in the direction of $S_{h\min}$. In general, holes drilled in normal faulting environments are fairly stable. Note that for an assumed overbalance of $\Delta P = 0.1\ S_v$, any rock with $C_0/S_v > 0.8$ would be expected to be stable, regardless of its orientation. In wells drilled to depths of 1-3 km, this means that boreholes of all orientations drilled in well-indurated sedimentary rocks would be stable, although poorly indurated rocks would not be for some orientations. From the perspective of determining what differential mud weight is needed to prevent borehole failure, very little differential mud weight ($\Delta P/S_v \sim 0.05$) is needed to inhibit failure, regardless of hole orientation.

Plates 3b and 3d show that as horizontal stress magnitudes increase, boreholes are more unstable. Considering the relationship between stress magnitude, rock strength, and borehole orientation, breakouts are expected in compressive stress environments even in relatively strong rock as comparisons of cases II, IV and VI demonstrate (the middle rows in Plates 2d, 3b, and 3d). In a near-vertical well bore in a normal faulting environment (II, Plate 2d) failure will occur in rocks where $C_0/S_v < \sim 0.4$, whereas in a strike-slip faulting environment (IV, Plate 3b), failure will occur in much stronger rocks where $C_0/S_v < 2.5$, and in a reverse environment (VI, Plate 3d), failure is expected even in rocks with normalized strength of $C_0/S_v < 3.3$. For an assumed rock strength of $C_0 = S_v$, no differential mud weight is required to stabilize the near-vertical hole for stress state II, a differential pressure of $\Delta P/S_v \sim 0.3$ is required in the case of stress state IV, and an extremely high differential pressure of $\Delta P/S_v \sim 0.45$ is necessary to prevent borehole failure for stress state VI. Note that this borehole fluid pressure would correspond to a drilling fluid with a density approximately equal to 0.9 of the density of the surrounding rock.

While hydrostatic pore pressure was assumed in the previous figures, Figure 4 illustrates the importance of in situ pore pressure on the tendency for breakouts to occur. It shows how the tendency for failure in the case II varies for three different pore pressures: hydrostatic ($P_p = 0.45\ S_v$), which is the same as in Plates 2c and 2d presented again for reference; moderate overpressure ($P_p = 0.7\ S_v$); and high overpressure ($P_p = 0.9\ S_v$). The breakout orientations and values of ΔP and C_0 in Figure 4 were computed under the assumption that increased pore pressure increases the magnitude of the minimum principal stress, $S_{h\min}$, according to the frictional law (3), whereas the magnitude of the intermediate principal stress, $S_{H\max}$, may not be affected as long as it is greater than $S_{h\min}$ (equation (3) does not control the intermediate stress). There are several somewhat surprising features in Figure 4. For example, as the pore pressure affects the ratio of the maximum and minimum principal stresses, both the orientation of borehole failure and the tendency for failure are markedly different for overpressured and hydrostatically pressured cases. For the overpressured cases, failures are expected to occur on the sides of the hole for all hole orientations. This suggests that a marked change in breakout orientation may be associated with abrupt changes in pore pressure for holes drilled at some orientations. Moreover, because high pore pressure reduces the principal stress differences ($S_{h\min}$ approaches S_v), holes are generally more stable as pore pressure increases. For example, for $C_0/S_v = 1.0$ (middle column), holes of all orientations are more stable as pore pressure increases, and even underbalanced holes are stable when $P_p = 0.9\ S_v$. The same thing is commonly, though not universally, true when looking at the problem from the perspective of rock strength. Even when

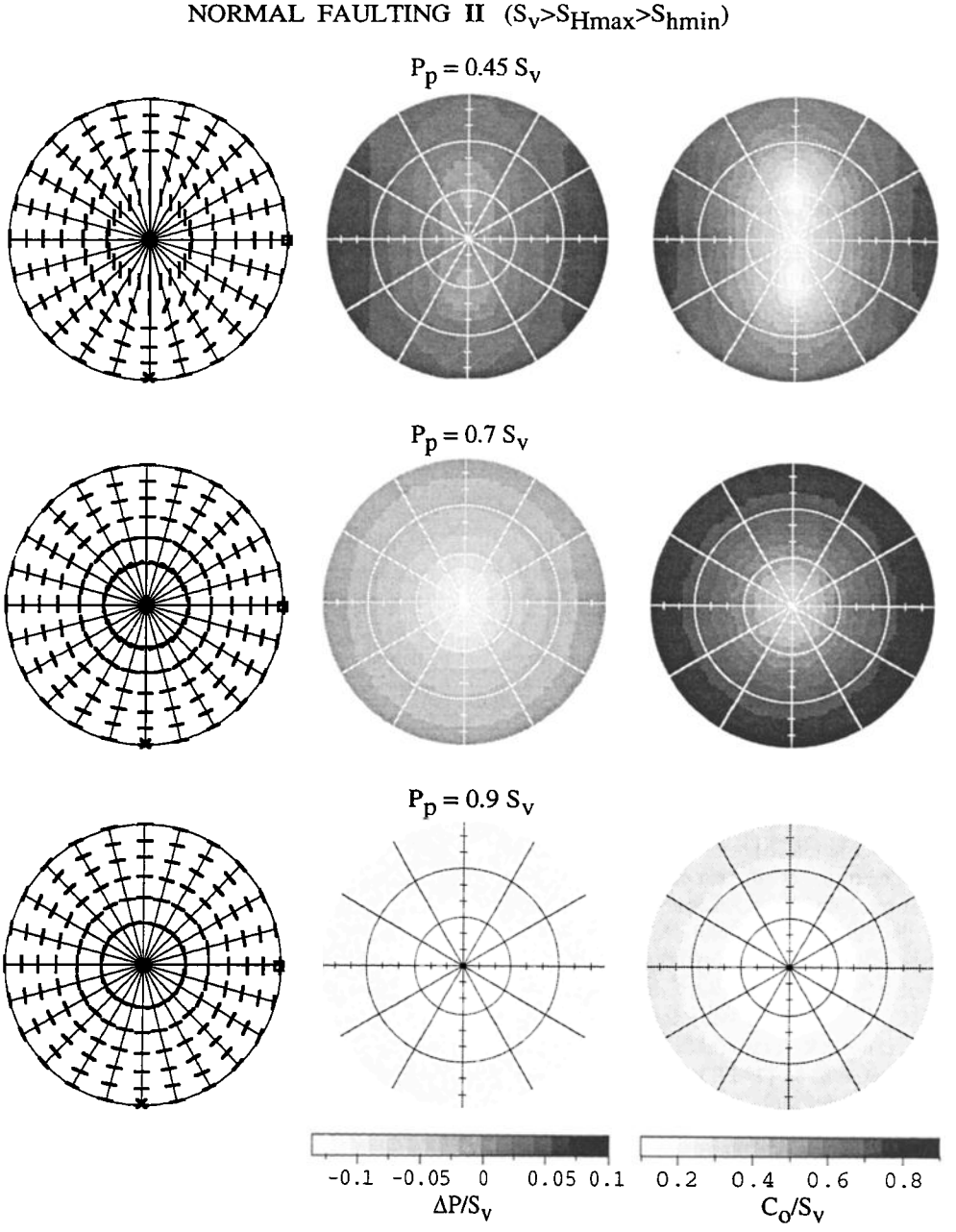

Figure 4. Effect of increased pore pressure on (left) breakout orientations and (middle) (right) tendency to fail for stress state II of Figure 3. The differential borehole fluid pressure, ΔP, is computed for $C_0 = S_v$ and $\mu_i = 1$ and the uniaxial rock strength, C_0, is computed for $\Delta P = 0.1\ S_v$ and $\mu_i = 1$. All values of stress are normalized by the vertical stress, S_v.

mud weights are small, $\Delta P/S_v = 0.1$ (right column), extremely weak rock is stable in holes of all orientations for $P_p = 0.9\ S_v$.

Many aspects of the tendency for boreholes to fail with increasing horizontal stress are intuitive. For example, one apparently obvious "rule of thumb" is that boreholes drilled parallel to the maximum principal stress are usually most stable. However, there are some interesting exceptions to this that are worth noting. When the maximum and intermediate principal stresses are equal (cases III and VII), for example, the most stable direction is actually in the direction of the least principal stress. The reason for this is that there are uniform stresses acting in the plane orthogonal to the borehole. Thus a more general rule of thumb is that the most stable orientation of the borehole is always in a plane perpendicular to the intermediate principal stress S_2 and rotates in this plane from the S_1 direction to the S_3 direction as S_2 varies in magnitude from S_3 to S_1. Applying this criterion to normal faulting as shown in Plate 2d, the most stable direction of drilling rotates in the plane perpendicular to the intermediate stress S_2=$S_{H\max}$ from the direction parallel to S_1=S_v to the direction parallel to S_3=$S_{h\min}$.

Tensile Wall Fractures in Deviated Boreholes

Tensile wall fractures for holes of various orientations are shown in Plate 4a using similar convention as used in Plate 2a.

Both the azimuth of the wall fracture measured around the borehole (the short blue lines) and the inclination of the wall fracture with respect to the hole axis (the short red lines) are referenced to the bottom side of the borehole (see Figure A2 for a full description). As two wall fractures occur on opposite sides of the borehole, the inclination of the wall fracture closest to the bottom side of the hole is shown. Axial tensile wall fractures (Plate 1a) are expected only when the red lines in the polar plots are parallel to the direction of borehole inclination (green radial lines of the polar net). If no red or blue lines are presented, it means that either the stress concentration computed around the hole has two extremes and the azimuth of tensile fractures is nonunique (Figure A3) or the stress around the borehole wall is uniform and the azimuth is not defined. We show below that these cases are fairly rare.

Plates 4b, 5a, and 5c illustrate the orientation of tensile wall fractures and Plates 4c, 5b, and 5d show the tendency for them to occur for the same seven stress states and hydrostatic pore pressures considered for breakouts. For simplicity, we assume that the tensile strength of the rock is zero (in effect we are assuming that failure will occur at a preexisting flaw or irregularity at an appropriate point around the borehole wall). Thus, we present no illustration of the tendency for failure to occur as a function of tensile strength although this could be incorporated in the analysis. The color in Plates 4c, 5b, and 5d corresponds to the differential mud weight just required to cause failure. Red represents cases for which little differential pressure is required to cause failure, whereas blue represents cases for which appreciable differential borehole fluid pressure is required for failure. The effect of the differential mud pressure is opposite for breakout and tensile fracture formation ("weighting up" the mud increases hole stability with respect to compressive failure but increases the likelihood of tensile failure; note the opposite sense of the color scales in Plates 2 and 3 and Plates 4 and 5). Since borehole fluid pressures cannot exceed the magnitude of the least principal stress, S_3 (hydraulic fracturing would occur in permeable rocks), we indicate the maximum borehole pressure possible for each case. In the above discussion related to inhibiting breakout formation by increasing mud weight (Plates 2 and 3) this was not a problem. In each case considered, the maximum borehole pressure considered was less than the least principal stress.

Plates 4b and 4c show the nature of tensile fracture initiation for normal faulting stress states I-III. Case I (when both horizontal stresses are equal and appreciably less than the vertical stress) indicates a large range of borehole inclinations for which the orientation of the tensile fractures is nonunique (see Appendix A). The large red regions in Plate 4c imply numerous borehole orientations for which tensile wall fractures should be a fairly common feature and Plate 4b indicates that these fractures are predicted to be inclined to the borehole axis. *Brudy and Zoback* [1993] showed that because nonaxial tensile wall fractures dip with respect to the borehole axis and propagate over only a relative narrow range of angles around the well bore, a number of these fractures form in succession and appear as "chevrons" as shown in Plate 1b. As in the case of the breakouts for stress cases II and III (Plate 2c), Plate 4b shows that there are azimuths for which the orientation of fractures changes abruptly as the hole inclination increases.

Tensile wall fractures are not expected for the borehole orientations indicated by the relatively "cool" colors in Plate 4c because these colors correspond to appreciable excess borehole fluid pressures that initiate hydraulic fractures with orientations that differ from those of wall fractures (orientation of an induced tensile fracture is expected to become more axial with an increase in borehole fluid pressure as the principal stresses in the borehole wall rotate into the direction parallel and perpendicular to the borehole axis; also *Mastin* [1988]). Thus the inclinations of the tensile wall fractures shown in Plates 4b, 5a, and 5c are those corresponding to only small $\Delta P/S_v$ (the regions shown in red); these wall fractures are likely to occur naturally only with little-to-no excess borehole pressure. Since differential borehole fluid pressures in excess of 0.18 S_v cannot be achieved (since these values would exceed the value of $S_{h\min}$), values of $\Delta P/S_v$ exceeding 0.18 in Plate 4c are theoretical values that cannot be achieved in practice.

For the case of the strike-slip fault environment (Plates 5a and 5b), tensile wall fracturing is expected for a limited range of borehole orientations for which differential borehole pressures are small. Axial fractures (short red lines in radial direction) are expected for a relatively narrow range of conditions. In general, the fractures should be inclined with respect to the well bore axis. The maximum values of $\Delta P/S_v$ for the three cases shown in Plate 5b are 0.18, 0.36, and 0.55, respectively.

For the case of the thrust fault environment (Plates 5c and 5d), tensile fracturing of the borehole wall at low differential mud weights is expected for a wide range of borehole orientations. Axial fractures are almost never seen (except for horizontal holes at some azimuths), and, in general, the tensile fractures in highly inclined boreholes strike in a direction orthogonal to borehole azimuth (radial pattern of short blue lines). The maximum value of $\Delta P/S_v$ is 0.55 for the three cases shown. Thus drilling-induced tensile fractures are not expected for near-vertical holes for stress cases VI and VII.

As for the breakouts, the same rule of thumb exists for the most stable orientations for the formation of tensile fractures (Plate 4c, 5b, and 5d); the most stable orientation is in the plane perpendicular to S_2 and rotates from S_1 to S_3 as S_2 increases from S_3 to S_1. Thus, for a given stress state, borehole orientations for which breakouts are expected are the same orientations for which tensile fractures are likely.

The orientation and tendency for occurrence of tensile wall fractures for different pore pressures in the case of stress state II are shown in Figure 5. The orientation and likelihood of failure are different for overpressured and hydrostatically pressured cases. However, in contrast to compressive failure (Figure 4), the tendency for tensile failure does not universally decrease as pore pressure increases; rather, changes in pore pressure affect stable and unstable borehole orientations. While for hydrostatic pore pressures the most stable holes are nearly horizontally in the direction of $S_{h\min}$, vertical boreholes are the most stable for highly overpressured rocks for this particular stress case.

A Case Study From the Gulf of Mexico

The figures presented above were provided for general illustration of the orientation and tendency for failure of inclined holes for various stress states. Obviously, if the stress state is known, these types of figures can be quite useful in determining the most stable borehole orientation. In this section we consider application of this theory to help constrain the magnitude and orientation of the far-field stress and rock strength. We propose a simple technique for field applications with the following generalized logic:

1. Utilize estimates of the least principal stress (from either leak-off tests or microfracture measurements), the overburden stress S_v, and the pore pressure P_p to construct a series of

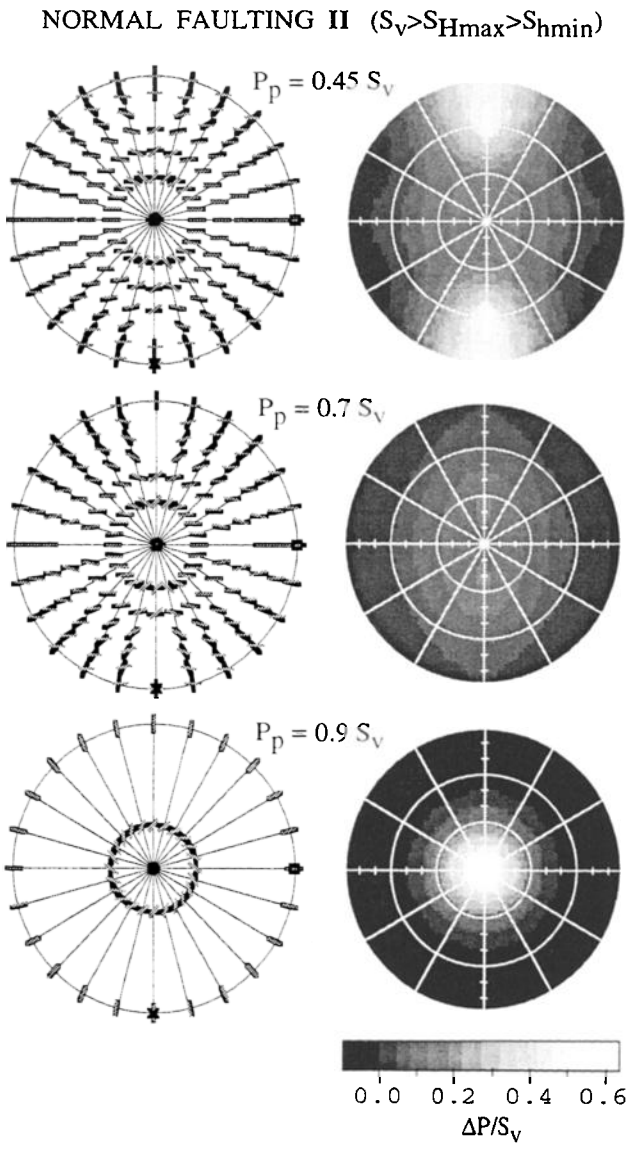

Figure 5. Effect of increased pore pressure on (left) orientations of tensile wall fractures and (right) tendency to fail for stress state II of Figure 3. Tendency for failure is expressed as a function of differential borehole fluid pressure, ΔP, which causes fracture initiation. Values of pressure are normalized by the vertical stress; zero tensile strength is assumed.

theoretical borehole failure diagrams (similar to Plates 2-5) for different states of stress. In the case of normal and strike-slip faulting, where the least principal stress corresponds to $S_{h\min}$, the only unknown stress is $S_{H\max}$.

2. Utilize observations of the breakouts and tensile wall fractures (from BHTV, dipmeter, FMS/FMI logs) to assess the orientation of the failures (and whether or not they are observed for the given mud weight) in light of the diagrams from the step above. Through this, one can determine the orientation and magnitude of $S_{H\max}$. Knowledge of the constitutive law for failure, rock strength, and elastic moduli is not required for this step to work. It is also not necessary to assume that one principal stress is vertical; however, to determine whether or not this assumption holds generally requires observations in multiple well bores.

3. Using information about stress magnitudes from the previous step, compressive failures are compared with the corresponding diagram for the tendency for failure to determine an upper bound estimate of effective in situ rock strength for intervals in which breakouts are present.

We demonstrate this methodology for a case study from the Gulf of Mexico. The Pathfinder well is an extension of the Pennzoil A-20ST production well in Eugene Island Block 330, offshore Louisiana. It was drilled in 1993 as a part of a Global Basins Research Network/Department of Energy/oil industry cost-sharing project into a growth fault with the primary target to test the hypothesis that the oil and gas can be produced from a fault zone which acts as a conduit to the reservoir [*Anderson et al.*, 1994].

The Eugene Island 330 field is a classic Gulf of Mexico minibasin [*Alexander and Flemings*, 1995] with a growth fault system at its northern boundary and a down-to-the-north fault zone at the southern boundary of the minibasin. The sediments filling the basin consist of alternating sequences of sands and shales that are likely floored by deep-water turbidites from the ancestral Mississippi River delta. As the growth fault zone accommodated extension toward the deep-water Gulf of Mexico, the sediments in the depobasin were folded into rollover anticlines that are now filled with oil and gas. Extension was caused by the withdrawal to the south of an extensive salt sill present near the surface. Hard geopressures separate the shallow shelf sands and shales from the deeper basin floor fan deposits because the high sedimentation rates and a thick, overlying deep-water shale produced permeabilities that are too low for the compacting pore fluids to escape.

Four-arm caliper measurements associated with an FMI log run in the Pathfinder well indicate systematic borehole enlargements from a depth interval 2158-2180 m, about 150 m above the growth fault zone. We interpret these enlargements to be breakouts because the borehole is not elongated in the direction of inclination (to distinguish apparent breakouts from possible key seats), the small diameter of the hole is the same as the bit size and the dipmeter arms were not rotating. At the depth of breakout detection, the borehole deviates 32° from the vertical at an azimuth N35°E and the breakouts form at angle θ_{cf} = 17°

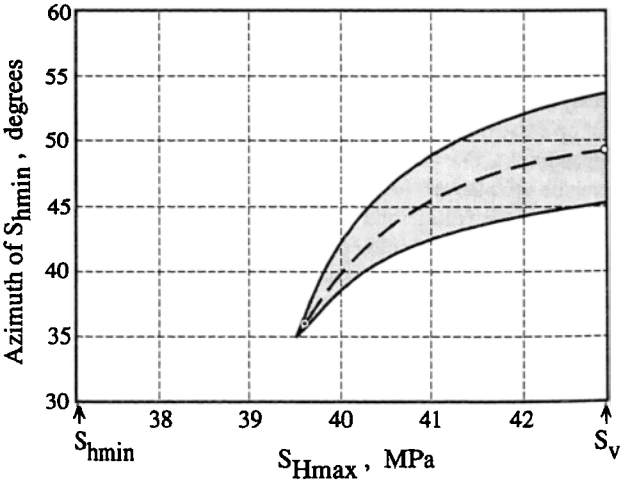

Figure 6. Magnitude of the maximum horizontal stress $S_{H\max}$ and azimuth of the minimum horizontal stress $S_{h\min}$ for which a breakout can form at an angle of 17° (± 5°) measured from the bottom side of a hole which is inclined 32° in the direction N35°E (S_v = 43.0 MPa, $S_{h\min}$ = 37.1 MPa, P_p = 29.0 MPa).

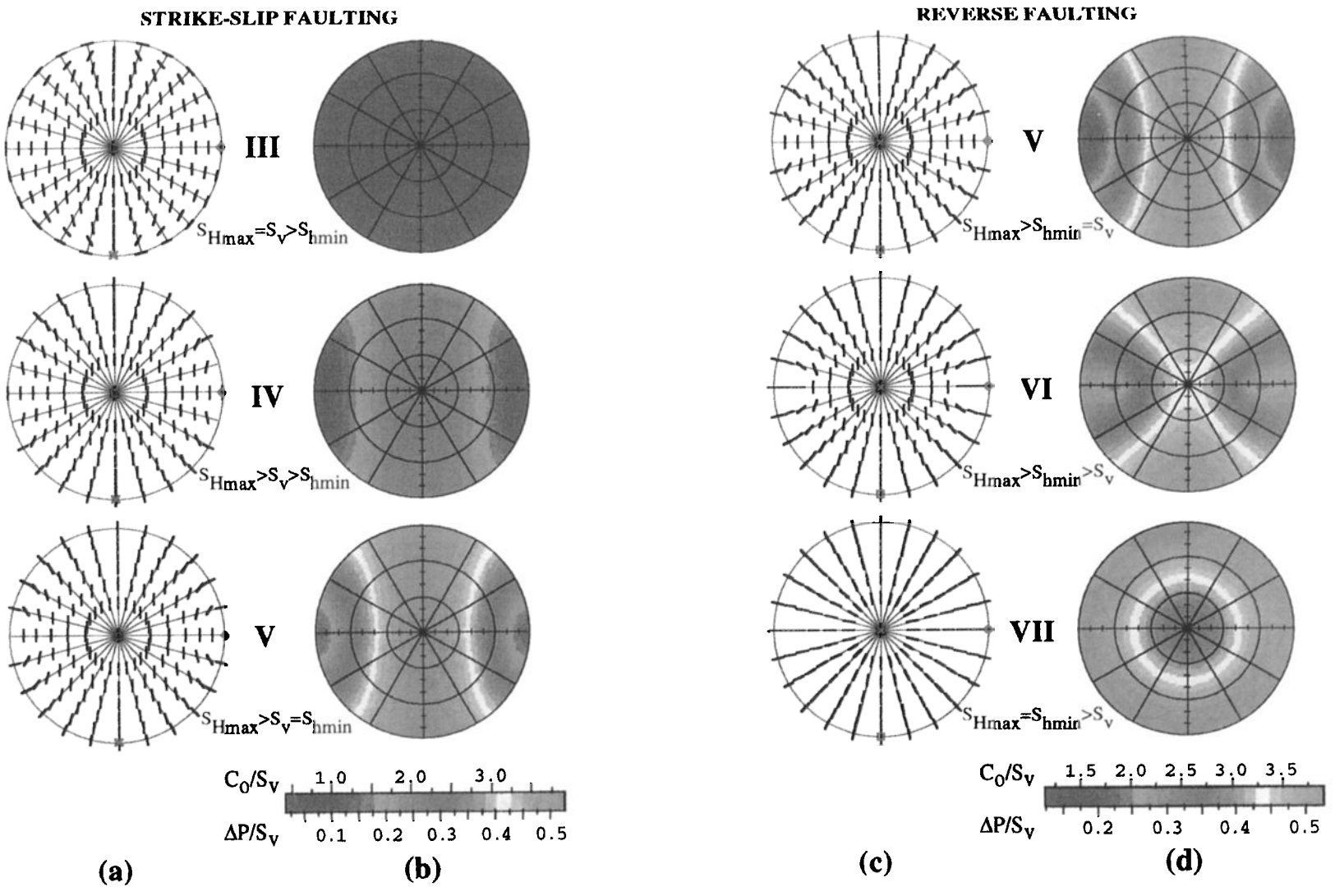

Plate 3. Breakouts in deviated boreholes for the strike-slip faulting (Plates 3a and 3b) and the reverse faulting (Plates 3c and 3d) stress regime. Stress states correspond to the states of stress III-VII of Figure 3. $S_{H\max}$ acts from left to right; $S_{h\min}$ acts from top to bottom at each polar plot. (a) (c) Breakout orientations are presented by the "looking down the hole" convention. (b) (d) Tendency for failure is expressed as a function of differential borehole fluid pressure, ΔP (computed for $C_0 = S_v$ and $\mu_i = 1$) or uniaxial rock strength, C_0 (for $\Delta P = 0.1\ S_v$ and $\mu_i = 1$) which is necessary to prevent borehole failure. Values of ΔP and C_0 are normalized by the vertical stress, S_v.

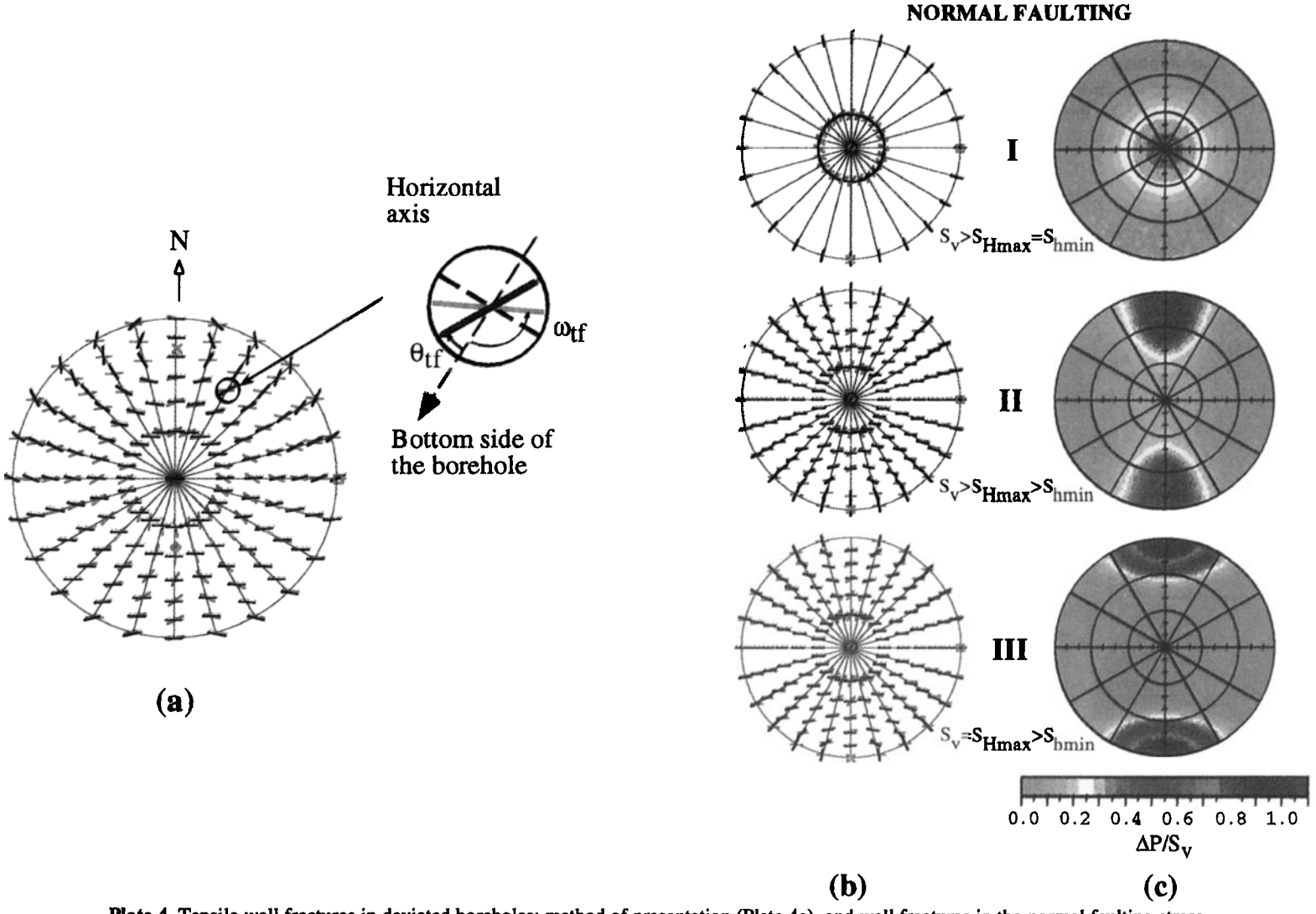

Plate 4. Tensile wall fractures in deviated boreholes: method of presentation (Plate 4a) and wall fractures in the normal faulting stress regime (Plates 4b and 4c). (a) Orientation of tensile wall fractures is plotted using the "looking down the hole" convention for boreholes of various orientations. The far-field stress is the same as in Plate 2a. The azimuth of failure, θ_{tf}, is measured clockwise from the bottom side of the hole in the plane perpendicular to the borehole axis; the inclination of wall fracture with respect to the hole axis, ω_{tf}, is indicated by an angle measured counterclockwise from the bottom side (see detail). (b) Orientations of tensile wall fractures for ΔP = 0 and (c) tendency for their occurrence in deviated boreholes in normal faulting stress states I-III of Figure 3. S_{Hmax} acts from left to right; S_{hmin} acts from top to bottom at each polar plot. The tendency for failure is expressed as a function of differential borehole fluid pressure, ΔP, which causes fracture initiation (given zero tensile strength).

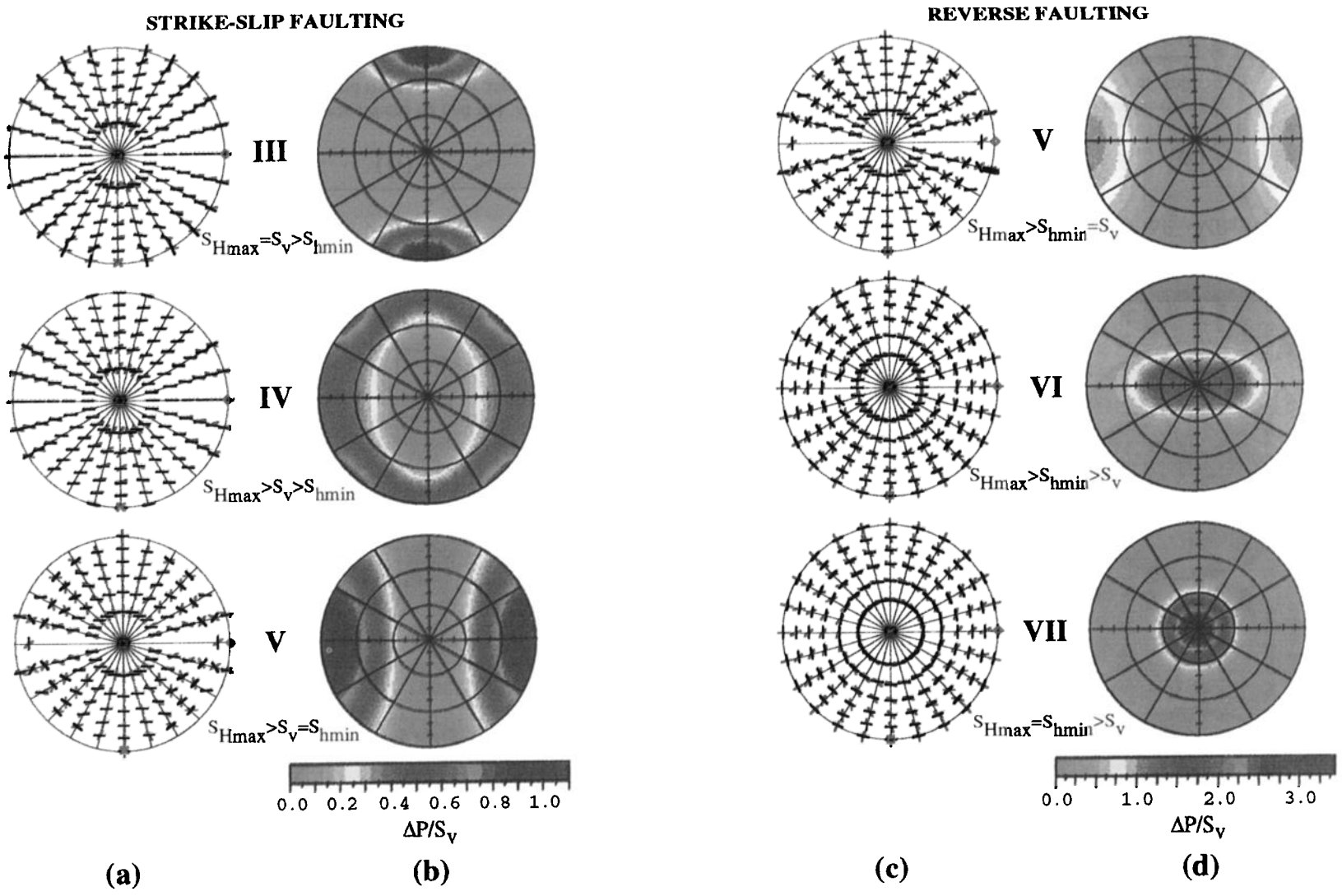

Plate 5. Tensile wall fractures in deviated boreholes for the strike-slip faulting (Plate 5a and 5b) and the reverse faulting (Plates 5c and 5d) stress regime. Stress states correspond to the states of stress III-VII of Figure 3. $S_{H\max}$ acts from left to right; $S_{h\min}$ acts from top to bottom at each polar plot. (a) (c) Fracture orientations are presented by the "looking down the hole" convention. (b) (d) Tendency for failure is expressed as a function of differential borehole fluid pressure, ΔP, which causes fracture initiation (given zero tensile strength). Values of ΔP are normalized by the vertical stress, S_v.

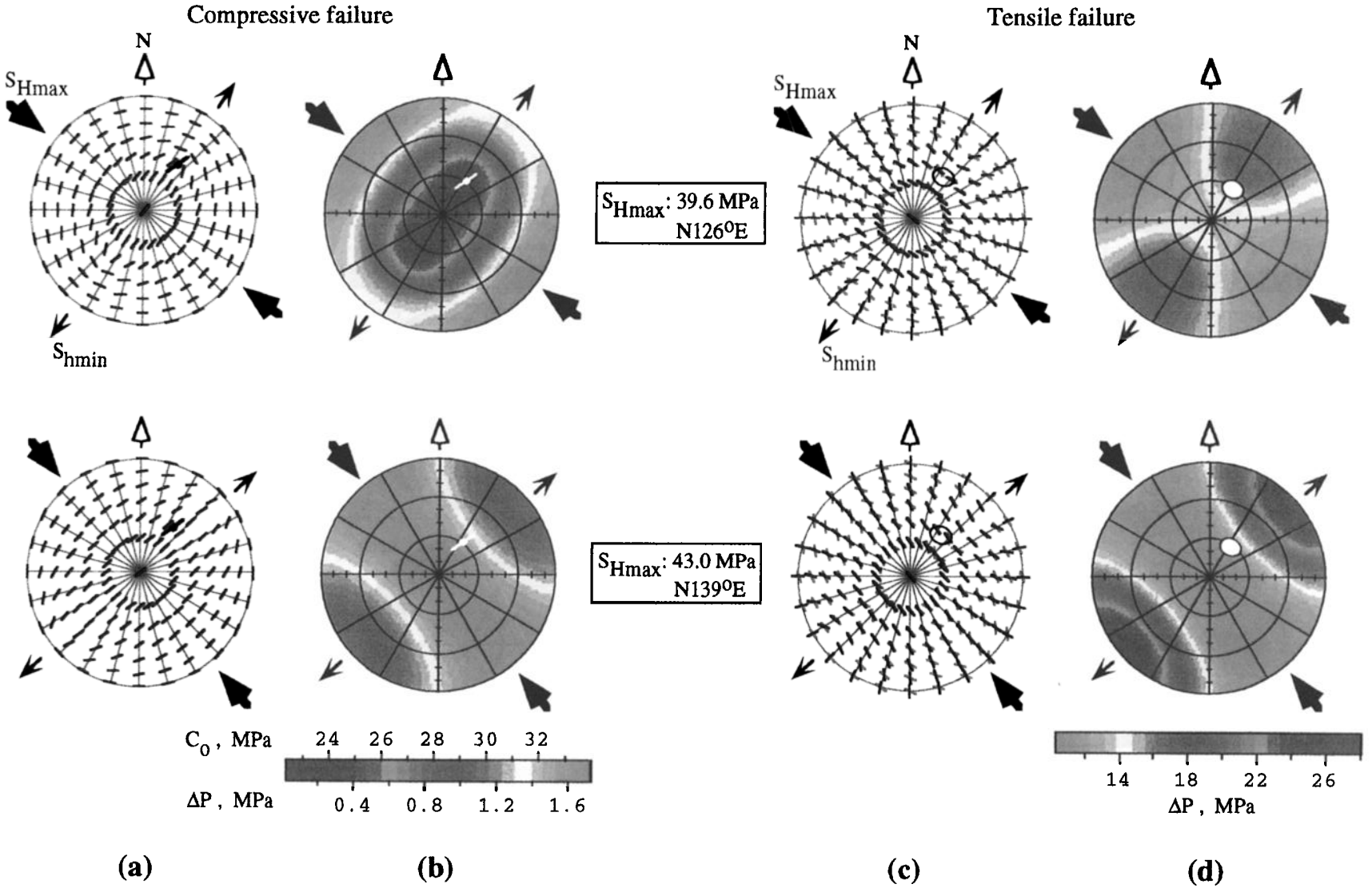

Plate 6. Borehole breakouts (Plates 6a and 6b) and tensile wall fractures (Plates 6c and 6d) in holes of various orientations for two limit states of S_{Hmax} inferred from breakout analysis in the Pathfinder well. (a) Orientations of breakouts and (c) orientations of wall fractures are computed for zero differential borehole fluid pressure ($\Delta P = 0$). (b) The tendency for failure by breakouts is expressed either as a function of uniaxial rock strength C_0 (for $\Delta P = 0$, $\mu_i = 1$) or as a function of ΔP (for $C_0 = 22.2$ MPa, $\mu_i = 1$) which is necessary to avoid borehole failure. (d) The tendency for tensile failure is shown as a function of ΔP which initiates wall fractures if zero tensile strength is assumed.

measured from the bottom side of the hole (at an azimuth of N55°E if projected onto a horizontal plane). A leak-off test from a depth of 2148 m provides an estimate of the least horizontal principal stress $S_{h\min}$ of 37.1 MPa. At this depth the vertical stress S_v is 43.0 MPa (computed from average density given by density log) and appears to be a principal stress as there are clear, naturally occurring vertical extension fractures in the FMI logs [*Anderson et al.*, 1994]. The pore pressure P_p is 29.0 MPa, which was estimated from mud weight and confirmed from laboratory compaction studies of the core [*Hart et al.*, 1995]. These observations represent information that is typically available in many offshore reservoirs. To fully determine the stress state, two stress components are still unknown: the magnitude of $S_{H\max}$ and the azimuth of $S_{h\min}$ (or azimuth of $S_{H\max}$).

Figure 6 indicates the magnitudes of $S_{H\max}$ and azimuths of $S_{h\min}$ which fit the observations. For values from the shaded region in Figure 6, a computed breakout azimuth (angle θ around the borehole for which $\sigma_{t\max}$ given by (A10) is the greatest) fits the observed azimuth of 17° with a tolerance of 5°. No other values satisfy the observations of breakouts and the known magnitudes of S_v, $S_{h\min}$, and P_p. The azimuth was computed for the magnitudes of $S_{H\max}$ and the azimuths of $S_{h\min}$ with steps of 0.1 MPa and 1°. As it is indicated by the dashed line for zero misfit in Figure 6, the azimuth of $S_{h\min}$ must be between N36°E and N49°E and the corresponding $S_{H\max}$ must have a value between 39.6 MPa and 43.0 MPa. Note that although it is commonly assumed that $S_{H\max} = S_{h\min}$ in the Gulf Coast, the $S_{H\max}$ value determined in this case departs significantly from $S_{h\min}$ and may be relatively close to S_v. Figure 7 shows that the direction of least horizontal compression is quite reasonable as it is orthogonal to the strike of the major growth fault passing through the hole just below the measurement depth.

To consider this case in the context of Plates 2-5, Plates 6a and 6b show theoretical breakout orientations and the tendency for breakout occurrence in deviated boreholes both for the lower bound estimate of $S_{H\max}$ (39.6 MPa at N126°E in the top row) and for the upper bound estimate of $S_{H\max}$ (43.0 MPa at N139°E in the bottom row). In both cases the azimuth of observed breakouts is different from the computed azimuth of $S_{h\min}$ (whereas in a vertical well the breakouts are at the same azimuth of $S_{h\min}$). Note that the occurrence of breakouts implies an effective uniaxial strength less than 22.2 MPa if $S_{H\max} = 39.6$ MPa and less than about 32 MPa if $S_{H\max} = 43.0$ MPa. These are reasonable values considering that the sediments in question are poorly indurated and clay-rich. Geochemical logging verified that the clay content of the shales above the main growth fault is greater than 40% [*Anderson et al.*, 1994]. If we take the conservative value of 22.2 MPa as an estimate of uniaxial strength, raising the mud weight only by 1.7 MPa (about 6% over the formation pore pressure) would be sufficient to prevent problems with well bore breakouts in boreholes of any orienta-

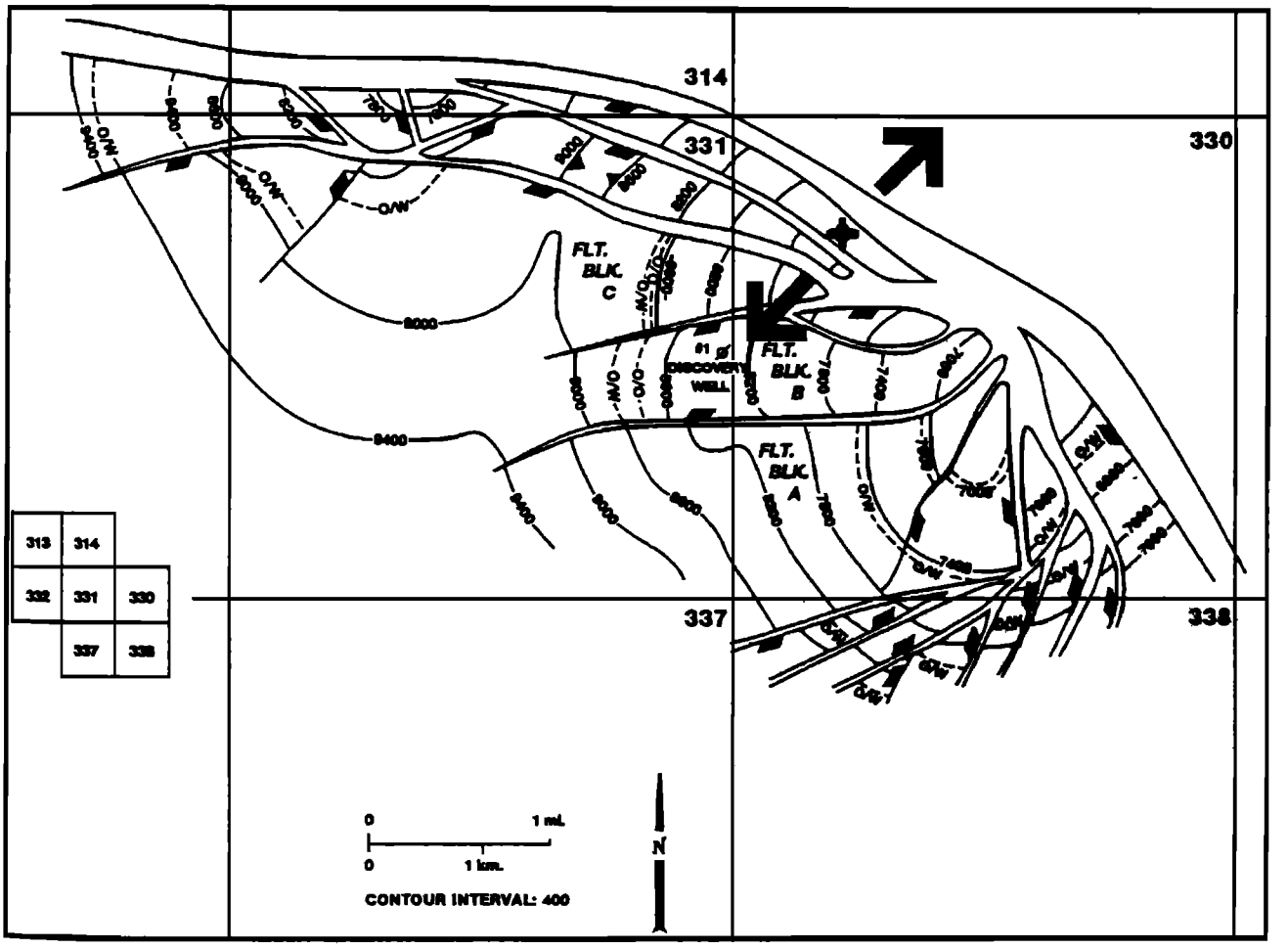

Figure 7. Top OI sandstone structure map [after *Holland et al.*, 1990, reprinted by permission] and direction of the least horizontal stress $S_{h\min}$ obtained from analysis of well bore breakouts.

tion in this stress field. A significant effect of the magnitude of $S_{H\max}$ is evident from Plate 6b. While in the first case the hole is drilled in an optimal direction with respect to the tectonic stress field, the hole is drilled in a relatively unstable orientation in the second case for which failure occurs even if rock strength is relatively high. Although no severe problems with breakouts occurred while drilling this well, drilling at the same azimuth, but at a great inclination, would have been more optimal.

Tensile wall fractures were not detected in FMS logs collected in this well. We can use this result as an internal check on the range of values of the magnitude of $S_{H\max}$ determined from the breakout analysis. Unfortunately, in this case, the lack of tensile wall fractures provides little additional information on the magnitude of $S_{H\max}$ because the differences between the three principal stresses are relatively small and there is little tendency for tensile failure to occur. Plate 6d shows that for the stress state existing at the site of the well bore, it would have taken an extremely high differential borehole pressure of approximately 12~16 MPa to have caused tension at the wall of a well bore with the orientation of the Pathfinder well.

Overall, this case may be representative of many field cases in which leak-off data provide an estimate of $S_{h\min}$, caliper data indicate the existence of some breakouts, pore pressure can be estimated, and the assumption that one principal stress is vertical seems valid. Optimally, multiple observations of well bore failure in a given area (optimally from several wells, or from different depths in the same well, which have different inclinations and/or azimuths) could be used to constrain the stress field.

Conclusions

In this paper we describe an analysis of the nature of compressive and tensile failures in arbitrarily inclined well bores under a wide variety of stress conditions that may be encountered in different parts of the world. This study indicates that the intermediate principal stress has a significant influence on the orientation of breakouts and tensile wall fractures and on borehole stability. For any state of in situ stress, it is straightforward to determine the orientation of the failures around any arbitrarily oriented well bore as well as to predict (as a function of rock strength and borehole fluid pressure) whether failure is likely to occur. We also show that this technique can be used to constrain in situ stress orientations and magnitudes and to assess effective in situ rock strength in any case of interest.

A simple application to well bore breakouts detected in the GBRN/DOE Pathfinder well, Gulf of Mexico, revealed that the magnitude of $S_{H\max}$ must be between 39.6 and 43.0 MPa and the azimuth of $S_{h\min}$ must be between N36°E and N49°E. No knowledge of either rock strength or elastic moduli was necessary for these determinations. Once the stress state was determined it was relatively straightforward to get upper bound estimates of the in situ rock strength between 22 and 32 MPa.

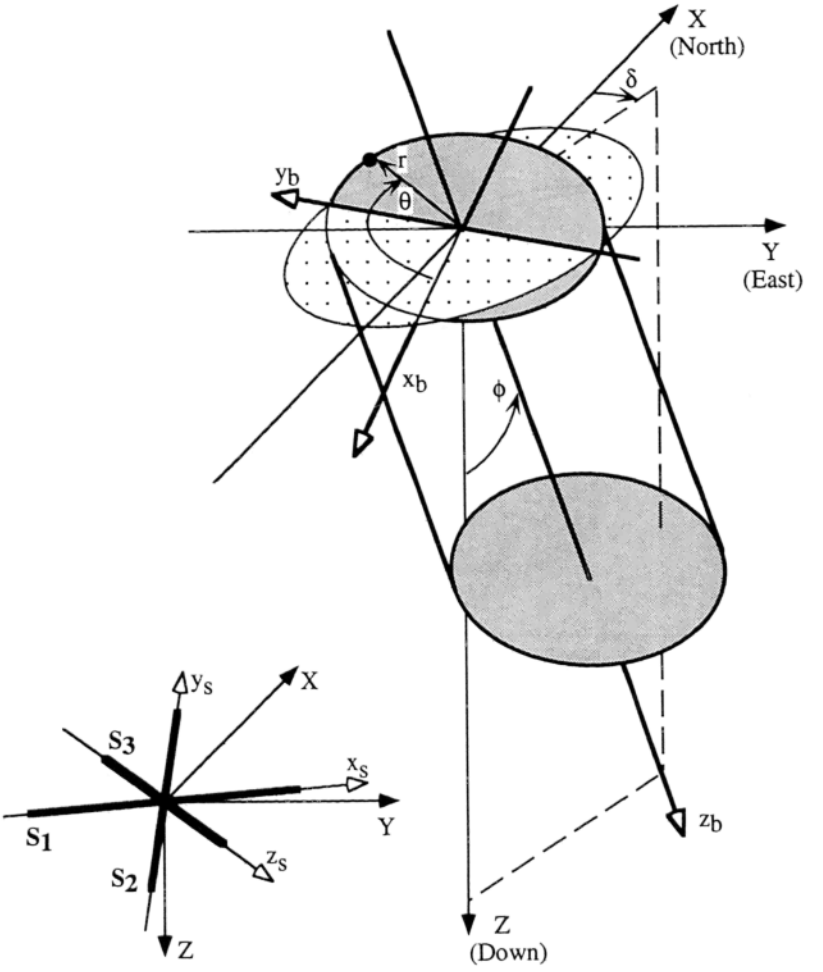

Figure A1. Borehole coordinate systems (x_b,y_b,z_b) and (r,θ,z_b) and a stress coordinate system (x_s,y_s,z_s) with respect to the geographic coordinates (X,Y,Z). The system (x_s,y_s,z_s) coincides with the far-field principal stresses S_1, S_2, S_3. The borehole orientation relative to the geographic coordinates is described by the azimuth δ and inclination ϕ..

Appendix A: Stresses at the Wall of an Arbitrarily Oriented Borehole

Let the far-field stress be expressed by means of the principal stresses S_1, S_2, and S_3 (Figure A1). Then the stress state is fully described by a tensor

$$\mathbf{S_s} = \begin{pmatrix} S_1 & 0 & 0 \\ 0 & S_2 & 0 \\ 0 & 0 & S_3 \end{pmatrix} \tag{A1}$$

where $S_1 > S_2 > S_3$ are principal stress magnitudes, and by three Eulerian angles α, β, γ defining the orientations of the principal stresses with respect to the geographic coordinate system.

The Eulerian angles α, β, γ define a sequence of three rotations necessary to rotate the geographic coordinate system (X,Y,Z) through systems (X',Y',Z') and (X'',Y'',Z'') to the system (x_s,y_s,z_s) where the axes x_s, y_s, and z_s coincide with the principal stresses S_1, S_2, and S_3. The rotation α ($0^o \le \alpha < 360^o$) is a positive rotation about the Z axis, the angle β ($-90^o \le \beta \le 90^o$) is a positive rotation about the new Y' axis, and the last angle γ ($0^o \le \gamma < 360^o$) is a positive rotation about the new X'' axis. For example, the Eulerian angles for the stress states from Plates 2-5 and Figures 4 and 5 ($S_{H\max}$ acts in the nominal "E-W" direction) are $\alpha = 0^o$, $\beta = 90^o$, $\gamma = 0^o$ for normal faulting (Plates 2c and 2d); $\alpha = 90^o$, $\beta = 0^o$, $\gamma = 90^o$ for strike-slip faulting (Plates 3a and 3b) and $\alpha = 90^o$, $\beta = 0^o$, $\gamma = 0^o$ for reverse faulting (Plates 3c and 3d). Mathematically, this transformation is

$$\begin{pmatrix} x_s \\ y_s \\ z_s \end{pmatrix} = \mathbf{R_s} \begin{pmatrix} X \\ Y \\ Z \end{pmatrix} \tag{A2}$$

where

$$\mathbf{R_s} = \begin{pmatrix} \cos\alpha\cos\beta & \sin\alpha\cos\beta & -\sin\beta \\ \cos\alpha\sin\beta\sin\gamma - \sin\alpha\cos\gamma & \sin\alpha\sin\beta\sin\gamma + \cos\alpha\cos\gamma & \cos\beta\sin\gamma \\ \cos\alpha\sin\beta\cos\gamma + \sin\alpha\sin\gamma & \sin\alpha\sin\beta\cos\gamma - \cos\alpha\sin\gamma & \cos\beta\cos\gamma \end{pmatrix}. \tag{A3}$$

Let any borehole geometry be expressed by means of two angles δ and ϕ, where δ is the azimuth of the horizontal projection of the borehole measured clockwise from the geographic north toward the east and ϕ is the deviation of the hole with respect to the vertical (Figure A1). If (x_b,y_b,z_b) is the local borehole coordinate system, where the z_b axis lies along the borehole axis (down positive), the y_b axis is oriented horizontally in the plane perpendicular to the hole axis, and the x_b axis is directed downward to the bottom side of the borehole, then the transformation of coordinates from the geographic system (X,Y,Z) to (x_b,y_b,z_b) is

$$\begin{pmatrix} x_b \\ y_b \\ z_b \end{pmatrix} = \mathbf{R_b} \begin{pmatrix} X \\ Y \\ Z \end{pmatrix} \tag{A4}$$

where

$$\mathbf{R_b} = \begin{pmatrix} -\cos\delta\cos\phi & -\sin\delta\cos\phi & \sin\phi \\ \sin\delta & -\cos\delta & 0 \\ \cos\delta\sin\phi & \sin\delta\sin\phi & \cos\phi \end{pmatrix}. \tag{A5}$$

On the basis of the transformation (A2), the given stress tensor S_s can be expressed in the geographic coordinate system (X,Y,Z) as

$$\mathbf{S_g} = \mathbf{R_s^T S_s R_s} \tag{A6}$$

and from (A6) and (A4) it follows that the far-field stress tensor in the local borehole coordinate system (x_b,y_b,z_b) is

$$\mathbf{S} = \mathbf{R_b R_s^T S_s R_s R_b^T}. \tag{A7}$$

Considering further only effective stresses,

$$\sigma_{ij} = S_{ij} - \delta_{ij} P_p \tag{A8}$$

where S_{ij} is a component of the tensor (A7) written in a matrix form, δ_{ij} is the Kronecker delta, and P_p is the pore pressure, the effective stresses at the borehole wall are given by formulas (first developed by *Hiramatsu and Oka* [1962] and checked by *Hayes* [1965]; later also *Fairhurst* [1968], for example)

$$\begin{aligned} \sigma_{zz} &= \sigma_{33} - 2\nu(\sigma_{11} - \sigma_{22})\cos 2\theta + 4\nu\sigma_{12}\sin 2\theta \\ \sigma_{\theta\theta} &= \sigma_{11} + \sigma_{22} - 2(\sigma_{11} - \sigma_{22})\cos 2\theta + 4\sigma_{12}\sin 2\theta - \Delta P \\ \tau_{\theta z} &= 2(\sigma_{23}\cos\theta - \sigma_{13}\sin\theta) \\ \sigma_{rr} &= \Delta P \end{aligned} \tag{A9}$$

where θ is the angle around the borehole wall measured from x_b to y_b, ν is Poisson's ratio (taken to be 0.25 in all computations), and ΔP is the difference between the borehole fluid pressure and the pore pressure in the rock.

The three principal stresses computed from the normal and shear stresses (A9) at the borehole wall are

$$\begin{aligned} \sigma_{t\max} &= \frac{1}{2}\left[\sigma_{zz} + \sigma_{\theta\theta} + \sqrt{(\sigma_{zz} - \sigma_{\theta\theta})^2 + 4\tau_{\theta z}^2}\right] \\ \sigma_{t\min} &= \frac{1}{2}\left[\sigma_{zz} + \sigma_{\theta\theta} - \sqrt{(\sigma_{zz} - \sigma_{\theta\theta})^2 + 4\tau_{\theta z}^2}\right] \\ \sigma_{rr} &= \Delta P \end{aligned} \tag{A10}$$

where $\sigma_{t\max}$ and $\sigma_{t\min}$ are the maximum and minimum effective stresses in the plane tangential to the borehole (Figure 2).

Figure A2 shows the principal stresses (A10) as a function of the azimuth θ around the hole for the particular borehole and stress state from Plate 2a. Given the axial symmetry of borehole stresses, only one half of the borehole wall (from the bottom to the top) is displayed. The maximum and minimum values of the principal stresses around the borehole define the azimuths θ_{cf} and θ_{tf} at which compressive or tensile failure could occur if the strength of the rock is exceeded. The angle ω_{tf} is the initial inclination of the fracture trace at the wall from the borehole axis (see stress crosses in Figure A2, the fracture propagates perpendicularly to $\sigma_{t\min}$).

Although the stresses around the borehole wall are periodic (with a period of π), they are not necessarily sinusoidal as a

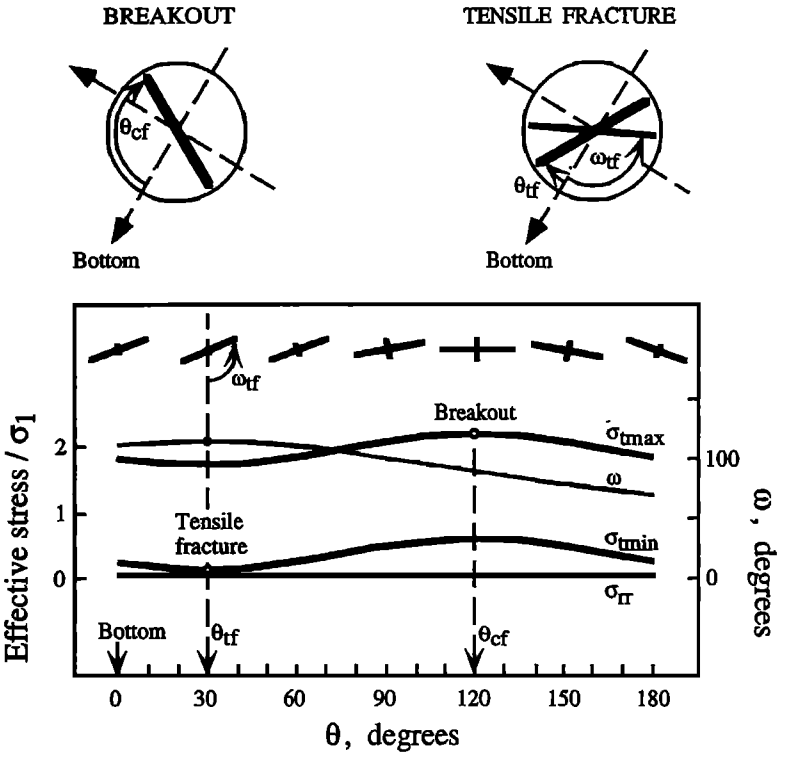

Figure A2. Principal stresses at the borehole wall as a function of the azimuth around the hole, θ, for the borehole orientation and in situ stress given in Plates 2a and 4a ($\delta = 45^{o}$, $\phi = 30^{o}$; $\sigma_1 = \sigma_2 = 3.12\ \sigma_3$, $\alpha = 0^{o}$, $\beta = 65^{o}$, $\gamma = 0^{o}$. The principal stress $\sigma_{t\max}$ deviates by angle ω from the hole axis (see the stress crosses). The azimuths of the maximum and minimum compressive stress define the orientations of the potential breakout (θ_{cf}) and the tensile wall fracture (θ_{tf}, ω_{tf}). These angles are also indicated in the top part of the figure in the same way as they are represented in the circular plots (see Plates 2a and 4a). All stresses are normalized by σ_1.

function of θ [*Mastin*, 1988], and there may be cases in which the tangential stresses have no unique extreme in the range of $0 \le \theta < \pi$ which means that the azimuth of failure is nonunique. This is illustrated in Figure A3 which shows the stress concentration at the wall of a borehole drilled in the direction of $S_{h\min}$ with an inclination of 45^{o} and subjected to the normal faulting stress state I of Figure 3. Two minima of $\sigma_{t\min}$ define two possible tensile wall fractures at azimuths of θ_{tf1} and θ_{tf2}. In addition, when there is a plane where the stress is uniform (plane in which principal stresses are equal), then stresses at the wall of a borehole drilled perpendicularly to this plane are uniform and the azimuth of failure is not defined at all (curves have no extremes as σ_{rr} in Figure A3).

Appendix B: Mohr-Coulomb Criterion for Compressive Failure

The Mohr-Coulomb failure criterion can be written in a general form

$$\sigma_1 = f(\mu_i)\sigma_3 + C_0 \qquad \text{(B1)}$$

where σ_1 and σ_3 are the maximum and minimum effective stresses, C_0 is the uniaxial strength [see *Jaeger and Cook*, 1979], and the function f,

$$f(\mu_i) = (\sqrt{\mu_i^2 + 1} + \mu_i)^2 \quad , \qquad \text{(B2)}$$

is a function of the coefficient of internal friction, μ_i. For most rocks, μ_i is in the range $1.0 < \mu_i < 2.0$.

Only two stresses explicitly enter the criterion (B1), but the yield surface is a three-dimensional irregular hexagonal pyramid in the principal stress space and when one of the principal stresses is constant, we can analyze 3-D failure conditions and yield surface in cross sections along planes $\sigma_{rr}=\Delta P$ as shown in Figure B1. (Note that when other failure criteria are considered,

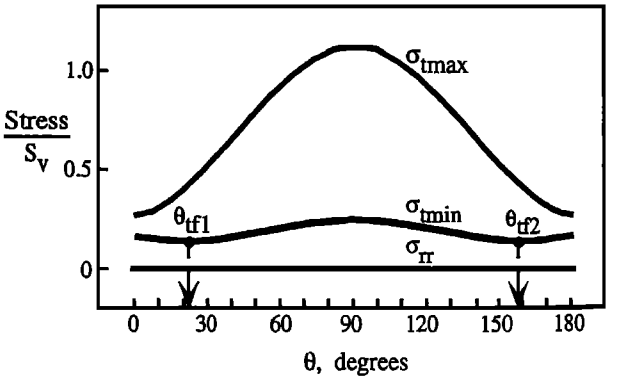

Figure A3. Illustration of the nonunique azimuth of a tensile wall fracture in a borehole inclined by 45^{o} in the direction of $S_{h\min}$ for the case of normal faulting stress state I of Figure 3. Two minima of the least tangential stress as a function of θ define two tensile fractures at azimuths of θ_{tf1} and θ_{tf2} around the borehole. Stresses are normalized by the vertical stress S_v.

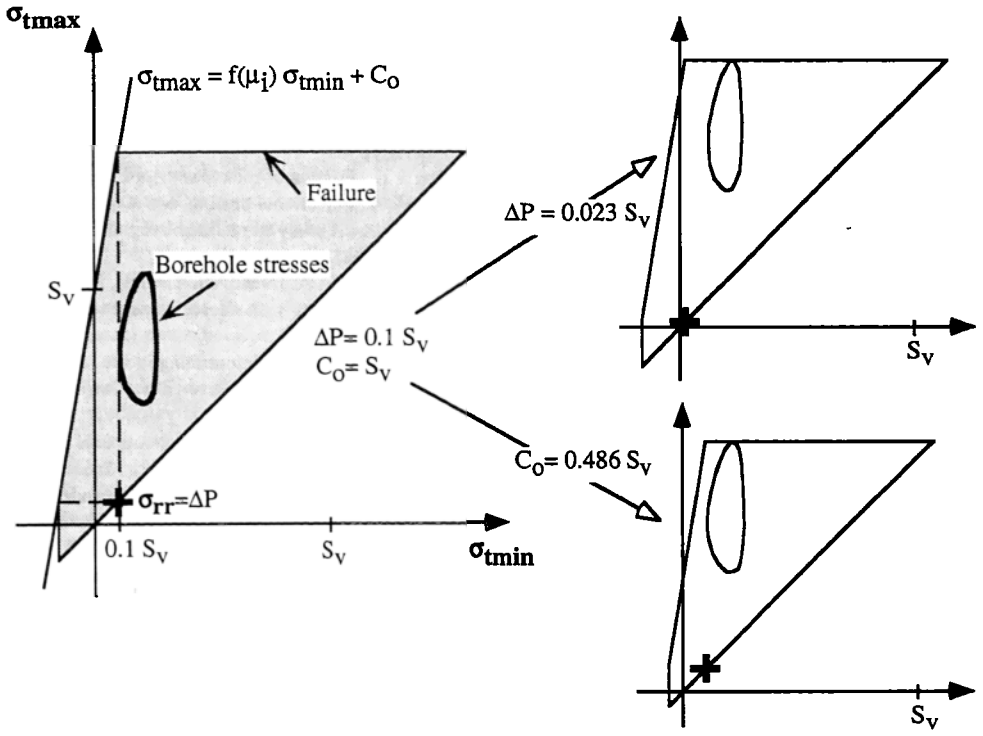

Figure B1. The Mohr-Coulomb failure polygon and principal stresses $\sigma_{t\max}$, $\sigma_{t\min}$, σ_{rr} at the borehole wall. The shaded region indicates allowable tangential stresses for the given frictional characteristics of the rock ($C_0 = S_v$, $\mu_i = 1$) and differential borehole fluid pressure ($\Delta P = 0.1\ S_v$). The solid curve within the polygon indicates all tangential stresses $\sigma_{t\max}$, $\sigma_{t\min}$ around the wall of an inclined hole ($\delta = 15^o$, $\phi = 60^o$) subjected to tectonic stresses (normal faulting stress state II of Figure 3). If the overpressure or rock strength decreases, the two pictures on the right illustrate the critical values ($\Delta P = 0.023\ S_v$ and $C_0 = 0.486\ S_v$) at which the borehole fails.

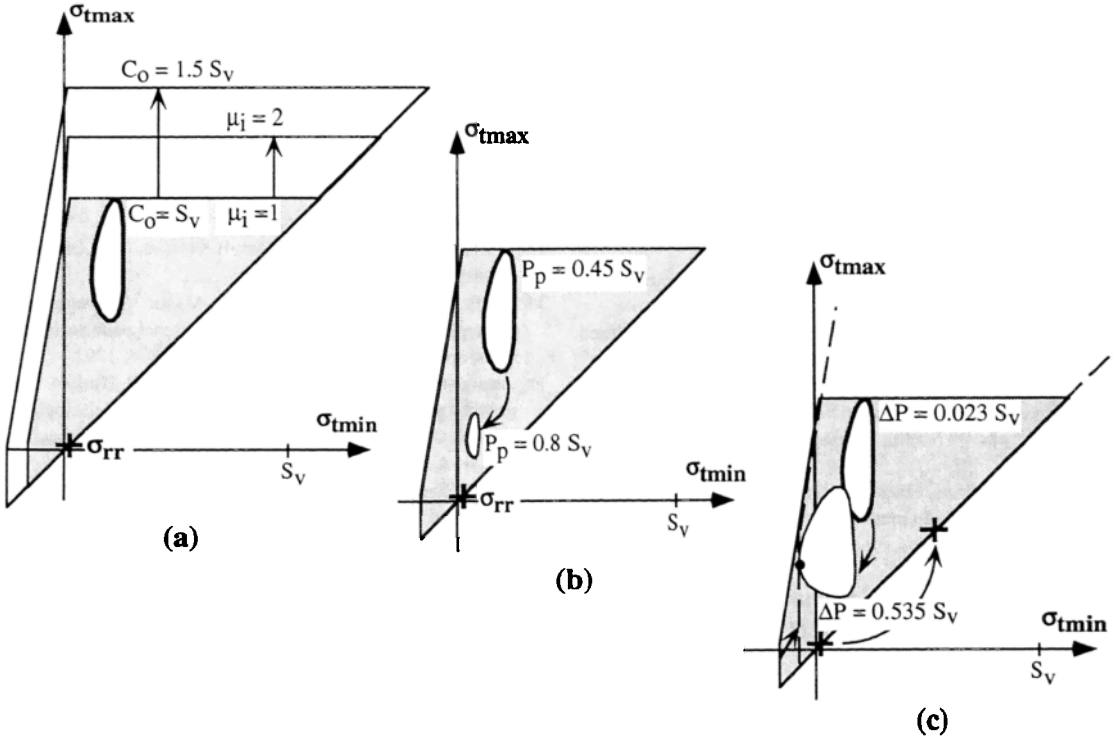

Figure B2. Effects of (a) frictional characteristics, (b) pore pressure, and (c) differential borehole fluid pressure on the compressive failure of an inclined borehole ($\delta = 15^o$, $\phi = 60^o$). The shaded Mohr-Coulomb polygon and heavy curve of the borehole stresses are the same as those shown in the top right corner of Figure B1 ($\Delta P = 0.023\ S_v$, $C_0 = S_v$, $\mu_i = 1$; normal faulting stress state II).

the hexagonal pyramid is replaced by yield surfaces of different shape and size; for example, by a simple cone in the case of the Drucker-Prager criterion). Since by definition $\sigma_{fmax} \geq \sigma_{fmin}$, only one half of the polygon is displayed. The visualization presented in Figure B1 is convenient to demonstrate how compressive failure is influenced by individual parameters. The failure conditions are determined by relative position of the polygon (borehole stresses allowable by the strength of the rock) and the curve of the tangential stresses at the borehole wall. Failure does not occur if the borehole stresses lie within the polygonal region of stresses allowable by strength characteristics of the rock, C_0 and μ_i. For the stress state chosen, Figure B1 also indicates how we determine the critical values of ΔP and C_0 at which failure is initiated. All values are normalized by the vertical stress and thus can be applied to any depth.

Figure B2a shows the effect of C_0 and μ_i values: the size of the polygonal region (or borehole stability) enlarges by increasing the uniaxial strength C_0 or the coefficient of internal friction μ_i. Note that the effect of μ_i is much smaller than that of C_0; an increase of μ_i from 1 to 2 is equivalent to a ~25% change of C_0. The increased pore pressure (Figure B2b) does not affect the polygon but shifts the curve toward the origin as the effective stresses are reduced. Thus the borehole is more stable in overpressured formations (assuming that ΔP is the same). The differential borehole pressure ΔP changes both the polygon and the curve (Figure B2c); higher borehole fluid overpressure makes the hole more stable in compression as it shifts the curve of borehole stresses away from the upper margin of the polygon. By increasing further the excess borehole fluid pressure, the curve may be forced to cross the marginal lines on the left (see the dot at the dashed polygon in Figure B2c).

Acknowledgments. We thank Roger Anderson and Peter Flemings of the GBRN project for their support and assistance with this work. Constructive reviews by Douglas Schmitt, Andreas Kronenberg, and Martin Brudy improved the quality of the manuscript. Financial support was provided by DOE grant DE-FC22-93BC14961 and NSF grant EAR-9209120.

References

Aadnoy, B. S., Inversion technique to determine the in-situ stress field from fracturing data, *J. Pet. Sci. Eng.*, *4*, 127-141, 1990a.

Aadnoy, B. S., In-situ stress direction from borehole fracture traces, *J. Pet. Sci. Eng.*, *4*, 143-153, 1990b.

Aadnoy, B. S., and M. E. Chenevert, Stability of highly inclined boreholes, *SPE Drill. Eng.*, 2, 364-374, 1987.

Adams, J., and S. Bell, Crustal stresses in Canada, in *The Geology of North America*, vol. 1, *Neotectonics of North America*, edited by D.B. Slemmons et al., pp. 367-386, Geological Society of America, Boulder, Colo., 1991.

Alexander, L., and P. Flemings, Hydrostratigraphy of the Eugene Island 330 mini-basin, *AAPG Bull.*, in press, 1995.

Anderson, E. M., The dynamics of sheet intrusion, *Proc. R. Soc. Edinburgh*, *58*, 242-251, 1937.

Anderson, R. N., P. Flemings, S. Losh, J. Austin, and R. Woodhams, In situ properties of a major Gulf of Mexico growth fault: Implications for behavior as a hydrocarbon migration pathway, *Oil Gas J.*, *92*(23), 97-104, 1994.

Baumgärtner, J., J. Carvalho, and J. McLennan, Fracturing deviated boreholes: An experimental laboratory approach, in *Rock at Great Depth, Proceedings ISRM-SPE International Symposium*, pp. 929-937, A. A. Balkema, Brookfield, Vt., 1989.

Bell, J. S., and D. I. Gough, Northeast-southwest compressive stress in Alberta: Evidence from oil wells, *Earth Planet. Sci. Lett.*, *45*, 475-482, 1979.

Bradley, W.B., Failure of inclined boreholes, *J. Energy Resour. Technol.*, *101*, 232-239, 1979.

Brudy, M., and M. D. Zoback, Compressive and tensile failure of boreholes arbitrarily-inclined to principal stress axes: Application to the KTB boreholes, Germany, *Int. J. Rock Mech. Min. Sci.*, *30*, 1035-1038, 1993.

Byerlee, J. D., Friction of rock. *Pure Appl. Geophys.*, *116*, 615-626, 1978.

Cooper, G. A., Directional drilling, *Sci. Am.*, *270*(5), 56-61, 1994.

Daneshy A. A., A study of inclined hydraulic fractures, *Soc. Pet. Eng. J.*, *13*, 61-68, 1973.

Ekstrom, M. O., C. A. Dahan, M. Y. Chen, P. M. Lloyd, and D. J. Rossi, Formation imaging with microelectrical scanning arrays, *Log Analyst*, *28*, 294-306, 1987.

Fairhurst, C., Methods of determining in situ rock stresses at great depths, *Tech. Rep. TRI-68*, Mo. River Div. Corps of Eng., Omaha, Nebr., 1968.

Gough, D. I., and J. S. Bell, Stress orientations from oil well fractures in Alberta and Texas, *Can. J. Earth Sci.*, *18*, 638-645, 1981.

Hart, B. S., P. B. Flemings, and A. Deshpande, Porosity and pressure: Role of compaction disequilibrium in the development of geopressures in a Gulf Coast Pleistocene Basin, *Geology*, *23*(1), 45-48, 1995.

Hayes, D. J., The in-situ determination of the complete state of stress in rock: The principles of a proposed technique, *CSIR Rep. MEG 404*, Counc. for Sci. and Ind. Res., Pretoria, South Africa, 1965.

Hiramatsu, Y., and Y. Oka, Stress around a shaft or level excavated in ground with a three-dimensional stress state, *Mem. Fac. Eng. Kyoto Univ.*, *XXIV*(I), 56-76, 1962.

Holland, D. S., J. B. Leedy, and D. R. Lammlein, Eugene Island block 330 field - U.S.A. offshore Louisiana, in *Structural Traps III: Tectonic Fold and Fault Traps, Atlas of Oil and Gas Fields*, compiled by E.Beaumont and N.Foster, pp. 103-143, American Association of Petroleum Engineers, Tulsa, Okla., 1990.

Jaeger, J. C., and N. G. W.Cook, *Fundamentals of Rock Mechanics*, 3rd ed., 593 pp., Chapman and Hall, New York, 1979.

Kirsch, G., Die Theorie der Elasticitaet und die Bedurfnisse der Festigkeitslehre, *VDI Z.*, *42*, 707, 1898.

Mastin, L., Effect of borehole deviation on breakout orientations, *J. Geophys. Res.*, *93*, 9187-9195, 1988.

Moos, D., and R. H. Morin, Observations of well bore failure in the Toa Baja well - Implications for the state of stress in the North Coast tertiary basin, Puerto Rico, *Geophys. Res. Lett.*, *18*(3), 505-508, 1991.

Moos, D., and M. D. Zoback, Utilization of observations of well bore failure to constrain the orientation and magnitude of crustal stresses: Application to continental, Deep Sea Drilling Project, and Ocean Drilling Program boreholes, *J. Geophys. Res.*, *95*, 9305-9325, 1990.

Moos D., and M. D. Zoback, State of stress in the Long Valley caldera, *Geology*, *21*, 837-840, 1993.

Müller B., M. L. Zoback, K. Fuchs, L. Mastin, S. Gregersen, N. Pavoni, O. Stephansson, and C. Ljunggren, Regional patterns of tectonic stress in Europe, *J. Geophys. Res.*, *97*, 11783-11804, 1992.

Papanastasiou, P., M. Thiercelin, J. Cook, and D. Durban, Behaviour and stability analysis of a wellbore embedded in an elastoplastic medium, in *Rock Mechanics*, edited by P. P. Nelson and S. E. Laubach, pp. 209-217, A. A. Balkema, Brookfield, Vt., 1994.

Peska, P., Breakout directions for deviated principal stress directions, *Acta Geod. Geophys. Mont. Hung.*, *28*(3-4), 343-351, 1994.

Plumb, R. A., and J. W. Cox, Stress directions in eastern North America determined to 4.5 km from borehole elongation measurements, *J. Geophys. Res.*, *92*, 4805-4816, 1987.

Plumb, R. A., and S. H. Hickman, Stress-induced borehole elongation: A comparison between the four-arm dipmeter and the borehole televiewer in the Auburn geothermal well, *J. Geophys. Res.*, *90*, 5513-5521, 1985.

Qian, W., and L. B. Pedersen, Inversion of borehole breakout orientation data, *J. Geophys. Res.*, *96*, 20093-20107, 1991.

Qian, W., K. S. Crossing, L. B. Pedersen, M. C. Dentith, and R. D. List, Corrections to "Inversion of borehole breakout orientation data" by Wei Qian and Laust Borsting Pedersen, *J. Geophys. Res.*, *99*, 707-710, 1994.

Rawlings, C. G., N. R. Barton, S. C. Bandis, M. A. Addis, and M. S. Gutierrez, Laboratory and numerical discontinuum modeling of wellbore stability, *J. Pet. Technol.*, *45*, 1086-1092, 1993.

Richardson, R. M., Hydraulic fracture in arbitrarily oriented boreholes: An analytic approach, in *Proceedings of a Workshop on Hydraulic Fracturing Stress Measurements, Dec. 2-5 1981*, pp. 167-175, National Academy Press, Washington, D. C., 1981.

Roegiers, J. C., and E. Detournay, Considerations on failure initiation in inclined boreholes, in *Key Questions in Rock Mechanics*, edited by P. A. Cundall et al., pp. 461-469, A. A. Balkema , Brookfield, Vt., 1988.

Stock, J. M., J. H. Healy, S. H. Hickman, and M. D. Zoback, Hydraulic fracturing stress measurements at Yucca Mountain, Nevada, and relationship to the regional stress field, *J. Geophys. Res.*, *90*, 8691-8706, 1985.

Veeken, C. A. M., J. V. Walters, C. J . Kenter, and D. R. Davies, Use of plasticity models for predicting borehole stability, in *Rock at Great Depth*, edited by V. Maury and D. Fourmaintraux, pp. 835-844, A. A. Balkema , Brookfield, Vt., 1989.

Vernik, L., and M. D. Zoback, Estimation of maximum horizontal principal stress magnitude from stress-induced well bore breakouts in the Cajon Pass scientific research borehole, *J. Geophys. Res.*, *97*, 5109-5119, 1992.

Yew, C.H., and Y. Li , Fracturing of a deviated well, *SPE Prod. Eng.*, *3*, 429-437, 1988.

Zajac, B., and J. M. Stock, Using borehole breakouts to constrain complete stress tensor, *Eos Trans. AGU, 73*(43), Fall Meeting suppl., 559, 1992.

Zoback, M. D., and J. H. Healy, Friction, faulting and in situ stress, *Ann. Geophys.*, *2*, 689-698, 1984.

Zoback, M. D., and J. H. Healy, In situ stress measurements to 3.5 km depth in the Cajon Pass scientific research borehole: Implications for the mechanics of crustal faulting, *J. Geophys. Res.*, *97*, 5039-5057, 1992.

Zoback, M.D., and M. L. Zoback, Tectonic stress field of North America and relative plate motions, in *The Geology of North America*, Decade Map vol. 1, *Neotectonics of North America*, edited by B. Slemmons et al., pp. 339-366, Boulder, Colo., 1991.

Zoback, M.D., D. Moos, L. Mastin, and R. N. Anderson, Well bore breakouts and in situ stress, *J. Geophys. Res.*, *90*, 5523-5530, 1985.

Zoback, M.D., R. Apel, J. Baumgärtner, M. Brudy, R. Emmermann, B. Engeser, K. Fuchs, W. Kessel, H. Rischmüller, F. Rummel, and L. Vernik, Upper-crustal strength inferred from stress measurements to 6 km depth in the KTB borehole, *Nature*, *365*, 633-635, 1993.

Zoback, M. L., First- and second-order patterns of stress in the lithosphere: The World Stress Map Project, *J. Geophys. Res.*, *97*, 11703-11728, 1992.

Zoback, M. L., and M. D. Zoback, State of stress in the conterminous United States, *J. Geophys. Res.*, *85*, 6113-6156, 1980.

Zoback, M. L., and M. D. Zoback, Tectonic stress field of the conterminous United States, *Mem. Geol. Soc. Am.*, *172*, 523-539, 1989.

Zoback, M. L. et al., Global patterns of tectonic stress, *Nature*, *341*, 291-298, 1989.

P. Peska and M. D. Zoback, Department of Geophysics, Stanford University, Stanford, CA 94305-2215. (e-mail: peska@pangea.stanford.edu; zoback@pangea.stanford.edu)

(Received August 8, 1994; revised January 19, 1995;
accepted January 26, 1995.)